Heliyon

ELSEVIER

Received:
17 September 2018
Revised:
21 January 2019
Accepted:
21 January 2019

Cite as: Linlin Xu, Danye Liu, Dong Chen, Hui Liu, Jun Yang. Size and shape controlled synthesis of rhodium nanoparticles. Heliyon 5 (2019) e01165. doi: 10.1016/j.heliyon.2019.e01165

Review Article

Size and shape controlled synthesis of rhodium nanoparticles

Linlin Xu [a,b], Danye Liu [a,b], Dong Chen [a,c], Hui Liu [a,c], Jun Yang [a,b,c,d,*]

[a] *State Key Laboratory of Multiphase Complex Systems, Institute of Process Engineering, Chinese Academy of Sciences, Beijing 100190, China*

[b] *University of Chinese Academy of Sciences, No. 19A Yuquan Road, Beijing 100049, China*

[c] *Center for Mesoscience, Institute of Process Engineering, Chinese Academy of Sciences, Beijing 100190, China*

[d] *Zhongke Langfang Institute of Process Engineering, Fenghua Road No 1, Langfang Economic & Technical Development Zone, Hebei Province 065001, China*

[*] Corresponding author.
E-mail address: jyang@ipe.ac.cn (J. Yang).

Abstract

Controlling of the size and/or shape of noble metal nanoparticles (NMNPs) is crucial to make use of their unique properties and to optimize their performance for a given application. Within the past decades, the development of wet-chemistry methods enables fine tailoring of the size and morphology of NMNPs. We herein devote this review to introduce the wet-chemistry-based methods for the size and shape-controlled synthesis of rhodium (Rh) NPs. We start with a summarization of the wet-chemistry-based approaches developed for producing Rh NPs and then focus on recent fascinating advances in their size- and shape-control in the aspects of kinetic and thermodynamic regimes depending on the synthetic conditions. Then, we use several typical examples to showcase the applications of Rh NPs with tunable sizes and shapes. Finally, we make some perspectives for the further research trends and development of Rh NPs. We hope through this reviewing effort, one can easily understand the technical bases for effectively designing and producing Rh NPs with desired properties.

https://doi.org/10.1016/j.heliyon.2019.e01165

Keywords: Nanotechnology, Materials chemistry, Physical chemistry

1. Introduction

Noble metal nanoparticles (NMNPs) with controlled sizes and shapes have increased scientific interest and technological significance owing to their unique physical/chemical properties and wide applications in catalysis, photonics, sensing, energy conversion/storage, and bio-medicine [1, 2, 3, 4, 5, 6, 7, 8]. Typically, the tunable sizes and shapes of NMNPs would determine their catalytic behavior in terms of activity, selectivity, and durability, through the adjustment of the number and geometric structure of the active sites [9, 10, 11, 12, 13]. In general, the high activity is associated with the large surface-to-volume ratio induced by small particle sizes. However, in some cases, the nanoparticles with appropriate bigger sizes may show better performance than that of the smaller ones. For example, Somorjai et al. demonstrated that the CO oxidation activity increases with the increase of the nanoparticle sizes, and 6-nm Ru NPs shows 8-fold higher activity than that of the 2 nm particles [14]. In addition, the intrinsic properties of most nanomaterials are also strongly dependent on their shapes [15, 16, 17, 18]. The catalytic performance is often attributed to the presence or absence of certain crystallographic planes associated with a particular shape, including exposed facets, as well as their associated atomic steps, corners, and defects [19, 20, 21]. Therefore, Engineering the size and shape of NMNPs is the keys to achieve their optimal performance for given technological applications.

Recently, significant progresses have been made for the size- and shape-control of NMNPs by tuning the crystal growth kinetics in numerous wet-chemistry approaches. Among various NMNPs, rhodium (Rh) is particularly known for its critical role in diverse catalytic reactions, such as CO oxidation [22, 23, 24, 25], NO reduction [26, 27, 28], hydrogenation [29, 30, 31, 32, 33], hydroformylation [34, 35, 36], and electro-oxidation [37, 38, 39, 40]. Moreover, Rh-based catalysts are especially stable for use under harsh reaction conditions because of its strong resistance to the etching of acid/base and heat. In order to maximize its catalytic performance, size- and shape-controlled synthesis of Rh NPs have obtained a wide range of researches in recent years [41, 42]. However, compared to other noble metals such as Au, Ag, Pt, and Pd, there are far fewer strategies reported on size- and shape-control of Rh NPs due to their extraordinarily high surface free energy [42]. Comprehensive review studies that summarize the synthetic methods of Rh NPs with size and shape control have also rarely been reported. Therefore, we intend to provide an overview to present the recent progresses in size- and shape-controlled synthesis of Rh NPs and their associated catalytic applications, with the majority of cited references from 2010 and afterwards.

https://doi.org/10.1016/j.heliyon.2019.e01165

In this review, we begin with an introduction of the wet-chemistry-based approaches developed for producing Rh NPs with tunable sizes and shapes, followed by their applications in various catalytic reactions. Finally, we make some perspectives for the further research trends and development of Rh NPs so as to provide the readers a systematic and coherent picture of this promising field.

2. Main text

2.1. Preparation methods for Rh NPs

The wet-chemistry methods are versatile towards the synthesis of different kinds of NMNPs, and both size and shape of NMNPs can be well controlled by manipulating the reaction kinetic and thermodynamic parameters. In recent years, the size and/or shape control of Rh NPs have been paid much attention by tuning the crystal growth kinetics in various wet-chemistry approaches, including modified polyol methods [15, 43], seeded growth methods [44, 45], organometallic approaches [46], electrochemical square-wave-potential routes [47], and template-directed methods [48, 49]. In this section, we emphasize a number of mainstream synthetic methods, and specific strategies for size/shape tailoring will be depicted in the next sections.

2.1.1. Synthesis of Rh NPs by polyol reduction

In recent years, a lot of research has been done on the formation of NMNPs using the polyol process, which is one of the most commonly used solution-based approaches to colloidal NMNPs for plasmonic and catalytic applications [50, 51, 52, 53, 54, 55, 56]. To produce a metal colloid, an organic metal compound or salt precursor is heated, usually in the presence of stabilizers, in high boiling polyols as solvents as well as reducing agents. Toshima and coworkers firstly reported their observation of a colloidal dispersion of branched Rh NPs in the late 1970s [57]. Rh NPs of 40 Å in diameter, which are effective for hydrogenation of cyclohexene, were prepared by refluxing the mixture of poly(vinyl alcohol) and $RhCl_3$ in methanol-water. Afterwards, liquid polyols have been proven to be suitable agents to reduce metal salts for the synthesis of monodispersed Rh particles with sizes in the nanometer scope.

As shown in Fig. 1, Xia et al. demonstrated the preparation of Rh multipods in large quantities by polyol reduction [15]. They also explored the influence of precursor concentration, reaction time, and temperature on the stability and morphology of Rh NPs. In a typical synthesis, ethylene glycol (EG) was placed in a three-necked flask equipped with a reflux condenser and a magnetic stirrer bar and heated in air (or Ar) at a designated temperature for 1.5 h. In separate vials, Na_3RhCl_6 and poly(-vinylpyrrolidone) (PVP) were each dissolved in EG at room temperature. The molar ratio of Na_3RhCl_6 to the repeating unit of PVP was controlled at 1:5. These two

https://doi.org/10.1016/j.heliyon.2019.e01165

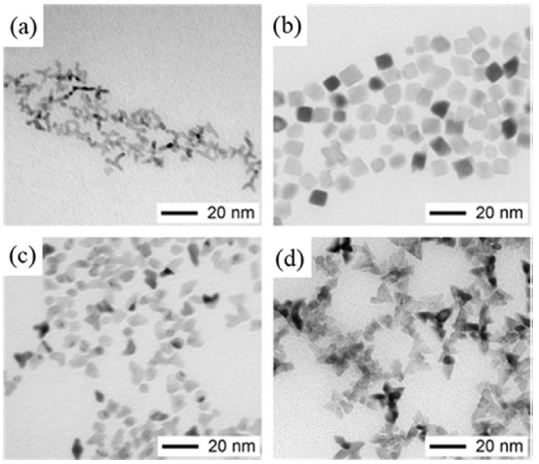

Fig. 1. TEM images showing the effects of temperature and the concentration of the precursor on the formation of branched Rh NPs: (a) 25 mM Na_3RhCl_6 at 110 °C, (b) 25 mM Na_3RhCl_6 at 180 °C, (c) 5 mM Na_3RhCl_6 at 140 °C, (d) 50 mM Na_3RhCl_6 at 140 °C (Adapted with permission from [15]. Copyright 2006, Wiley-VCH).

solutions in EG were injected simultaneously into the heated EG using a syringe pump at a rate of 0.2 mL min^{-1} for the formation of Rh NPs.

Recently, Schaak et al. modified the polyol synthesis and achieved the synthesis of nanometer sized Rh cubes, icosahedra, and triangular plates using bromide, trifluoroacetate, and chloride ligands, respectively [58], as shown in Fig. 2. Taking the heat-up synthesis of Rh icosahedra from molecular precursors as an example, the Rh precursors and PVP stabilizer were dissolved in polyol solvent using a 65 °C water bath, and $NaCOOCF_3$ [8:1 ratio with $Rh_2(COOCF_3)_4$] was also added. The mixed solution was stirred vigorously in a three-necked flask containing a condenser and septum, and the temperature was maintained using a digital controller. The solution was heated to a temperature for 15 min at which particle nucleation begins, as evidenced by a darkening of the color. Then the solution was heated to a focusing temperature for 75 min, causing the solution color to darken further, indicating the formation of Rh NPs with desired morphologies.

Combining microwave irradiation with polyol reduction can form a typical strategy for the synthesis of Rh NPs. Compared with conventional heating ways, microwave-assisted heating results in more uniform nucleation and shorter crystallization time, which is conducive to the formation of uniform metal colloids. Humphrey et al. conducted a comparative study to show the effects of microwave versus conventional heating on the nucleation and growth of near-monodispersed polymer-capped Rh NPs [59]. Extensive studies on formation of Rh NPs reveal fundamental differences during the nucleation phase that is directly dependent on the heating method; microwave irradiation was found to provide more uniform seeds for the subsequent growth of larger nanostructures of desired size and surface structure. Nanoparticle growth

https://doi.org/10.1016/j.heliyon.2019.e01165

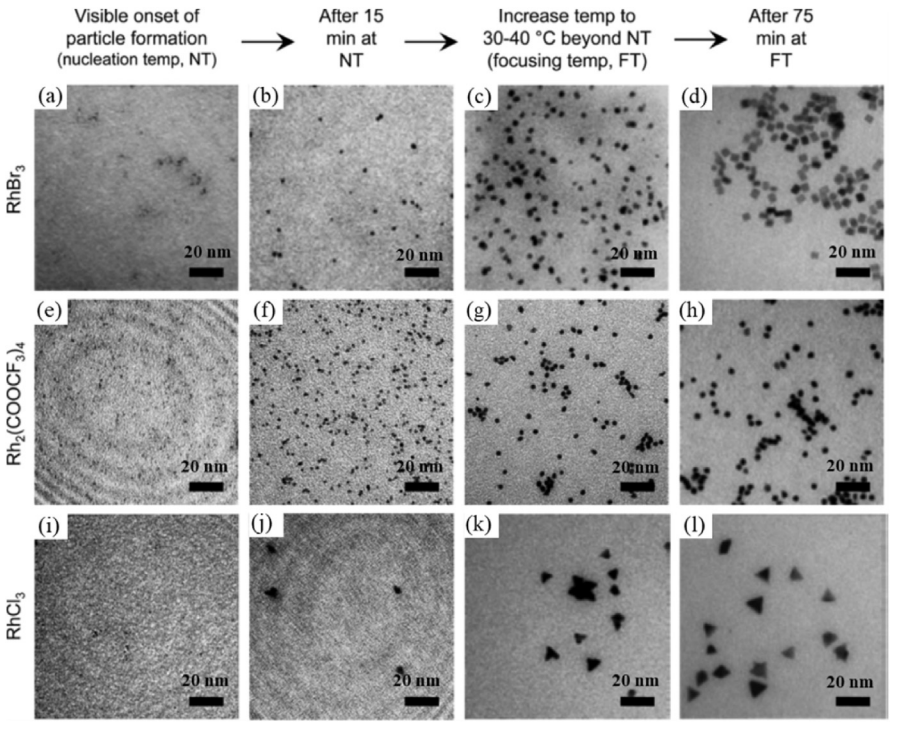

Fig. 2. TEM images showing aliquots taken during the heat-up synthesis of Rh cubes from $RhBr_3$ in DEG (a−d), icosahedra from $Rh_2(COOCF_3)_4$ in EG (e−h), and triangular plates from $RhCl_3$ in TREG (i−l). Aliquots were collected at (a, e, i) the temperature corresponding to the visible onset of particle nucleation, (b, f, j) after 15 min maintaining that temperature, (c, g, k) upon increasing the temperature 30−40 °C, and (d, h, l) after 75 min of focusing at that temperature (Adapted with permission from [58]. Copyright 2015, American Chemical Society).

kinetics is also markedly different under microwave heating. While conventional heating generally yields particles with mixed morphologies, microwave synthesis consistently provides a majority of tetrahedral particles at intermediate sizes (5−7 nm) or larger cubes (≥8 nm) upon further growth. High-resolution transmission electron microscopy (HRTEM) indicates that Rh seeds and larger nanoparticles obtained from microwave-assisted synthesis are more highly crystalline and faceted versus their conventionally prepared counterparts. Microwave-prepared Rh NPs also show approximately twice the catalytic activity of similar-sized conventionally prepared particles, as demonstrated in the vapor-phase hydrogenation of cyclohexene.

2.1.2. Synthesis of Rh NPs by seed-mediated growth

Seed growth method is a promising two-step process that separates thermally disfavored nucleation processes from subsequent spontaneous growth steps by adding monomers to existing nanoparticles [60, 61]. It has been employed for the growth of large metallic nanoparticles on seeds of the same metal and proved to be able

https://doi.org/10.1016/j.heliyon.2019.e01165

to synthesize a variety of metal nanoparticles. In the presence of stabilizers, seed particles may be generated due to the rapid reduction of metal precursors at elevated temperatures or metal precursors after the reduction may deposit on the seed surface.

Tilley et al. reported the radial anisotropic growth of Rh multipods that results from a homogeneous seeded growth mechanism [44]. Small Rh seeds were synthesized by reducing $RhCl_3$ in ethylene glycol in the presence of PVP. Then the Rh seeds were used to form larger Rh NPs without isolation. Subsequently, they reported the size-tunable synthesis of Rh cuboctahedra and multipod nanoparticles with mean diameters ranging between 3 and 7 nm by seeded growth from isotropic PVP-capped Rh seed clusters of 2.9 nm under specific and controlled reaction conditions [45]. The particle formed *via* control of the monomer addition rate was demonstrated in Fig. 3, and the intrinsic solvent viscosity was demonstrated to be a highly influential factor on particle shape.

2.1.3. Synthesis of Rh NPs by decomposing organometallic precursors

The organometallic derivatives, e.g. $Rh(acac)_3$, are widely used as precursors for the synthesis of monodispersed Rh NPs [22, 62, 63]. One typical synthetic procedure using organometallic precursors for preparing Rh NPs is reported by Son and co-workers [46]. They successfully synthesized near-monodispersed Rh NPs with different morphologies by this approach and the key of the strategy was use of relatively unstable compounds 1−3 (Fig. 4) as precursors for the formation of nanoparticles at low temperature. In a typical synthesis, a suitable compound was added to well-dried oleylamine and the temperature rises gradually to a target temperature

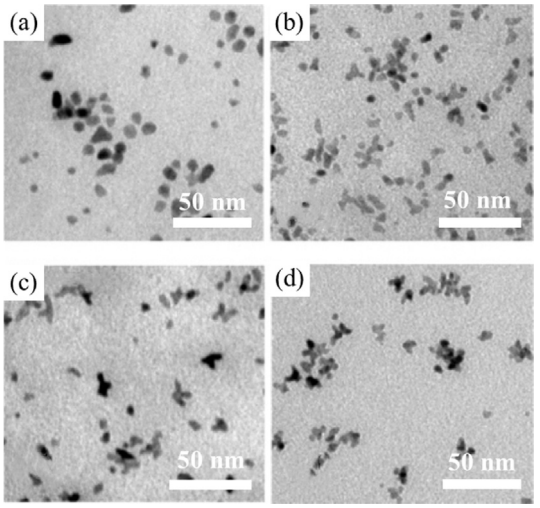

Fig. 3. Rh NPs prepared by addition of $RhCl_3$ to Rh-PVP seeds in 1,2-propanediol at (a) 10 mg h^{-1}, (b) 40 mg h^{-1}, (c) 160 mg h^{-1}, (d) jigsaw piece-shaped particles obtained for all monomer addition rates in 1,2-butanediol (Adapted with permission from [45]. Copyright 2007, American Chemical Society).

https://doi.org/10.1016/j.heliyon.2019.e01165

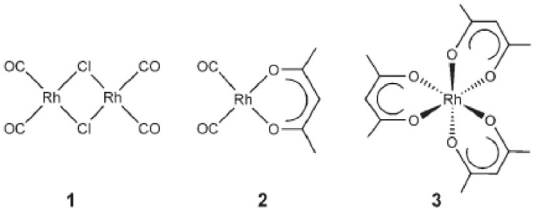

Fig. 4. Three different organometallic derivatives (compounds 1−3) used in the reaction for the synthesis of Rh NPs with different morphologies (Adapted with permission from [46]. Copyright 2007, Wiley-VCH).

(170 °C for tetrahedral, 190 °C for spherical and 220 °C for irregular, respectively) with vigorous stir. Then this reaction temperature was maintained for 1 h. In the process, the mixed solution changes from red to black. After the reaction, methanol was poured to form black precipitates, which were purified to obtain Rh NPs (Fig. 5).

2.2. Size control of Rh NPs

The size of NMNPs has a great influence on their catalytic performance [29, 64, 65]. In general, the most obvious dimension-related feature is that as the diameter decreases, the percentage of the surface atoms increases, and thus the catalytic performance is enhanced. However, the ratio of surface atoms is not the only factor determining the relationship between Rh particle size and catalytic performance.

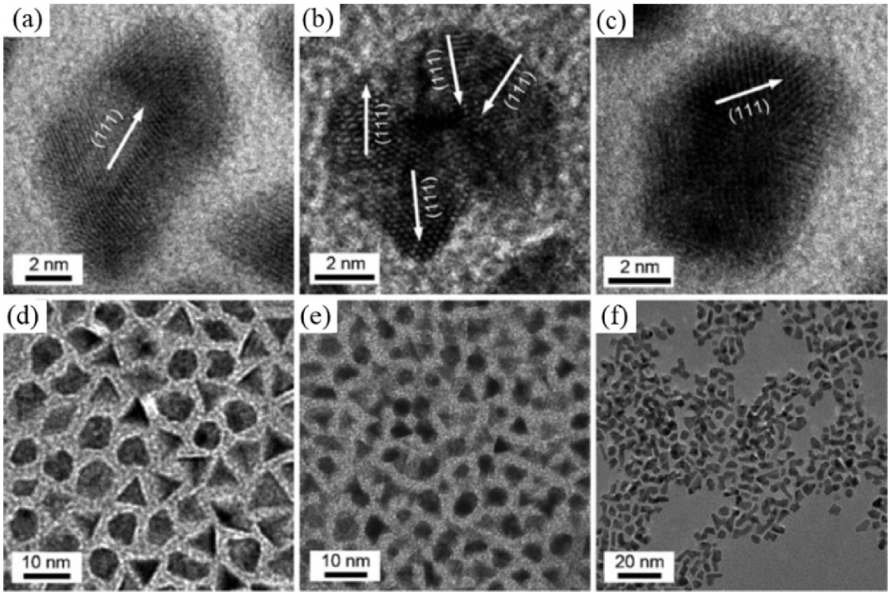

Fig. 5. Selected HRTEM images (a−c) of the particles in (d), (d) TEM image of the mixture of tetrahedral and spherical Rh NPs formed at 190 °C from precursor 1, (e) TEM image of the mixture of tetrahedral and spherical Rh NPs formed at 190 °C from precursor 2, (f) TEM image of rectangular rhodium nanoparticles formed at 220 °C by injection of precursor 3 into the hot solution (Adapted with permission from [46]. Copyright 2007, Wiley-VCH).

https://doi.org/10.1016/j.heliyon.2019.e01165

In fact, distinct surface activities are often observed for the particles with comparable sizes. The size effect of the nanoparticles can be attributed to several factors, such as changes in geometric structures, size dependent chemical properties and surface states [29].

Liu et al. recently reported the size-tunable Rh nanostructures for wavelength-tunable ultraviolet plasmonics [66]. The uniform monodispersed Rh NPs with edge lengths of 15−59 nm have been successfully and controllably synthesized with the use of slow-injection polyol methods (Fig. 6). The size of Rh NPs is mainly determined by the ratio of Rh seeds to injected Rh precursors. In their study, they synthesized unprecedented large Rh nanocubes with slight concave faces. In order to prepare the large size Rh NPs, they controlled the concentration of the generated Rh atoms in the low saturation state, and added enough Rh precursors to minimize the formation of the seeds, so that the seeds would grow into larger seeds. And poly-dispersed size-controlled Rh NPs they synthesized show a good prospect for ultra-violet (UV) plasmonics with tuning surface plasmon resonances.

In addition to the influence of the precursors, polymer stabilizers can also control the size, shape, and/or composition of the Rh NPs [67, 68]. Somorjai et al. reported the preparation of small polymer-stabilized Rh NPs with a narrow size distribution [22]. The size dependence was studied by in situ ambient-pressure X-ray photoelectron spectroscopy (APXPS). Fig. 7 shows some characterization results of Rh NPs. TEM images of particles with different sizes and their size distribution histograms can be seen in Fig. 7a−e. Fig. 7f illustrates X-ray photoelectron spectra (XPS) data for the Rh 3d peak of the as-synthesized particles without pretreatment after Langmuir-Blodgett deposition onto a silicon wafer, and the ratio of oxidized Rh to reduced Rh clearly increases as the particle size decreases. They also employed

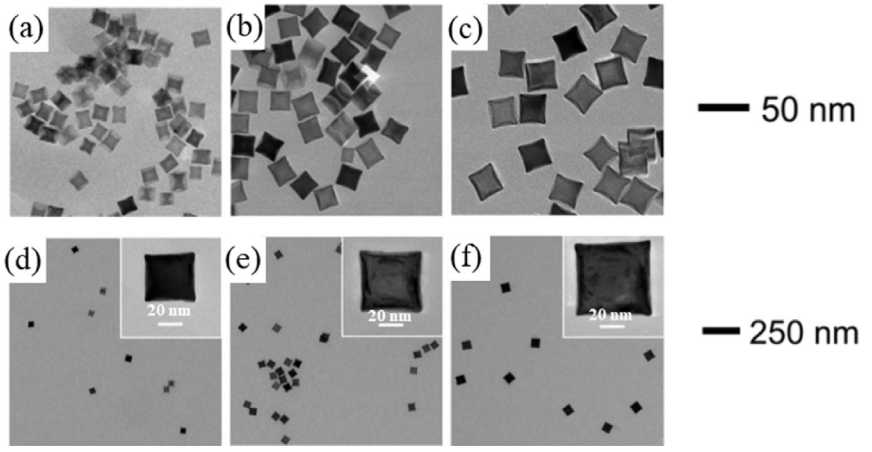

Fig. 6. TEM images of monodispersed Rh NPs in ethanol from slow-injection methods, with corresponding average edge lengths of 15 nm (a), 21 (b), 27 nm (c), 39 nm (d), 47 nm (e), and 59 nm (f), respectively (Adapted with permission from [66]. Copyright 2016, Royal Society of Chemistry).

https://doi.org/10.1016/j.heliyon.2019.e01165

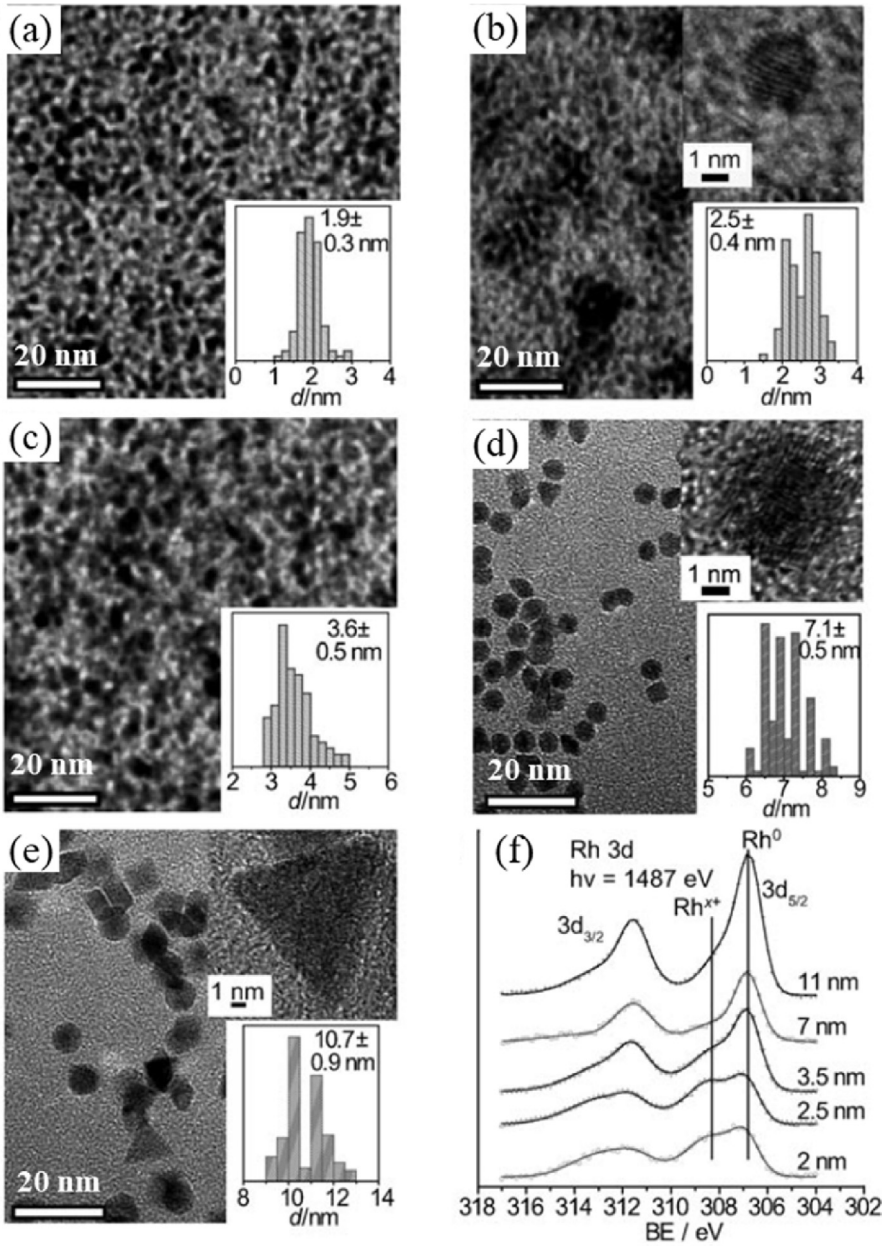

Fig. 7. TEM images with insets of particle size distribution histograms of 100 particles for (a) 2 nm, (b) 2.5 nm, (c) 3.5 nm, (d) 7 nm, and (e) 11 nm Rh NPs, (f) Rh 3d XPS spectra of these Rh NPs (Adapted with permission from [22]. Copyright 2008, Wiley-VCH).

a reactive oxide overlayer on Rh NPs with different sizes for CO oxidation to determine the effects of sizes on the catalytic performance.

Controlling the stabilizers during synthetic reaction process is another effective approach to tune the size of Rh NPs. Claver et al. reported the design and synthesis of 1,3-diphosphite ligands derived from carbohydrates and then used them as chiral nanoparticle stabilizers [69]. They were inspired by the studies demonstrating that

https://doi.org/10.1016/j.heliyon.2019.e01165

these ligands were selected owing to their successful enantioselective discrimination in several catalytic processes [70]. The TEM images were shown in Fig. 8, which display small mean sizes and narrow size distributions. Furthermore, they applied the Rh NPs with distinct sizes as catalysts for the asymmetric hydrogenation of the prochiral monocyclic arenes m-methylanisole and o-methylanisole. These Rh NPs are shown to be active, and the systems yield high cis-selectivity.

In order to achieve better practical application, researchers have made great efforts to regulate the size of Rh NPs. From the participating perspective in the synthesis of Rh NPs, the effective regulation of nanoparticle size can be realized through tailoring the stabilizers, precursors, ligands and other aspects involved in the reaction.

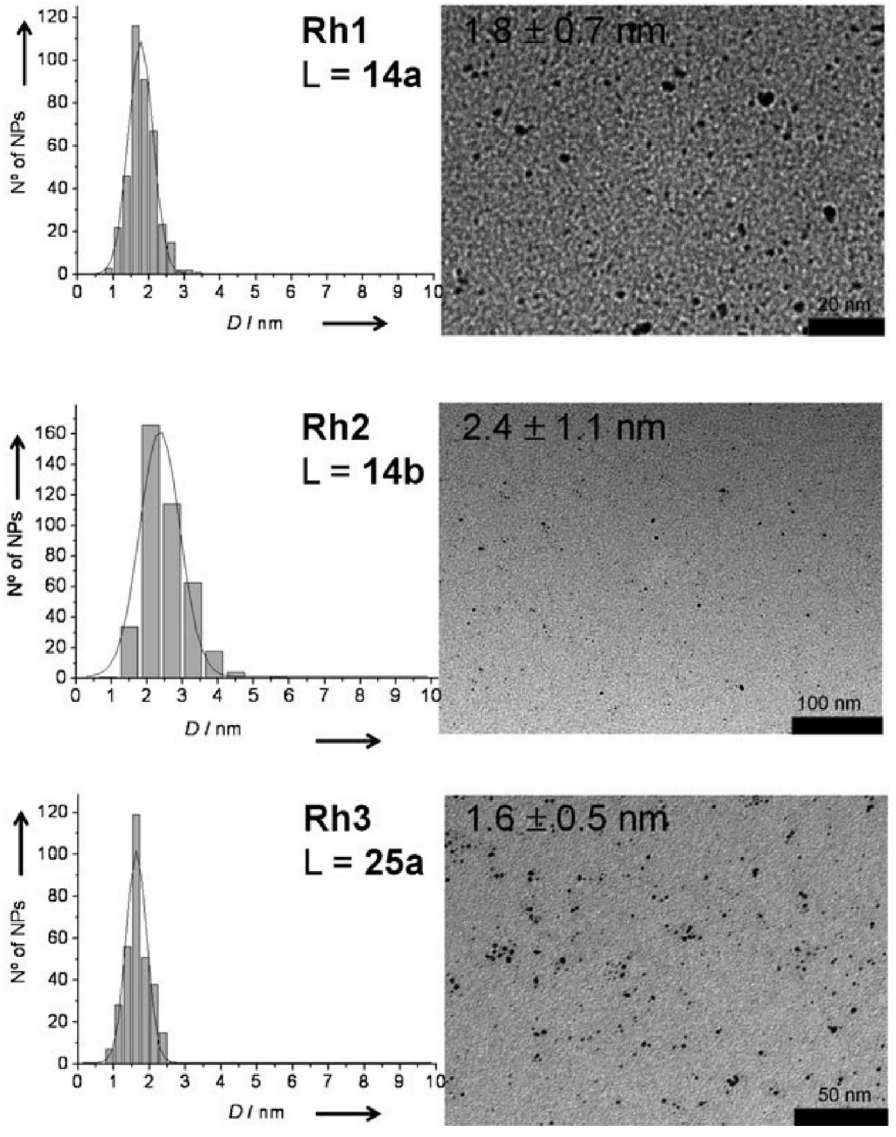

Fig. 8. TEM images and size distribution histograms for different Rh nanoparticles (Adapted with permission from [69]. Copyright 2009, Wiley-VCH).

https://doi.org/10.1016/j.heliyon.2019.e01165

2.3. Shape control of Rh NPs

To establish a correlation between the shape and catalytic performance of nanoparticles, a variety of different morphologies have been obtained for Rh NPs including cubes [43, 71, 72], decahedra [73], octahedral [21, 74], tetrahedral [46], sphere [75], multipods [15, 76, 77], and hexagonal polyhedral [25].

2.3.1. Synthetic approaches for spherical Rh NPs

NMNPs with spherical morphology are the most common products formed using solution-based methods. It is believed that spherical nanoparticles are thermodynamically stable, and therefore even harsher conditions could be used.

Schaak et al. presented the first example of Rh nanostructures formed by self-aggregation of small Rh particles [75]. They established the synthesis of PVP-stabilized Rh NPs, which spontaneously aggregate into dense spherical nanostructures in solution, and they studied the influence of polymer-surfactant mixtures on the morphology. Though reducing aqueous $RhCl_3$ solution with $NaBH_4$ in the presence of PVP, the spherical aggregates are yielded within the size range of 10−100 nm, which are built from smaller 1−3 nm Rh particles and form without the need for seed-mediated or electrochemical growth. The dense nanostructures are thermally stable, and they have a tendency to form ordered superstructures upon drying, as shown in Fig. 9. This system supports spontaneous hierarchical organization over three length scales, which suggests that more complex nanostructures may be accessible by optimizing the synthesis and purification processes to achieve higher monodispersity. These well-defined nanoparticle aggregates could be important systems for studying the influence of catalytic activity and cooperative magnetic properties on interparticle separation and nanostructure, since aggregated structures have proven to exhibit enhanced properties relative to those of their discrete nanoparticles and bulk powders.

To compare the shape-dependent catalytic activity of different types of nanoparticles, Son et al. also prepared spherical Rh NPs by hot injection method [46], as shown in Fig. 10 for their TEM images. Specifically, a solution of precursor (0.050 g, 0.12 mmol or 0.24 mmol) in oleylamine (4 mL) was rapidly injected into 6 mL hot oleylamine at 250 °C. The reaction mixture was stirred for 1 h at 250 °C, and then cooled down to room temperature and washed by methanol twice. The obtained precipitates were dried under vacuum for two hours and dispersed in 10 mL of hexane.

2.3.2. Synthetic approaches for polyhedral Rh NPs

For Rh NPs, the form of polyhedron is very common in the process of morphology control, such as cube, octahedron, tetrahedron, hexagon, decanedron and tetrahexahedron.

https://doi.org/10.1016/j.heliyon.2019.e01165

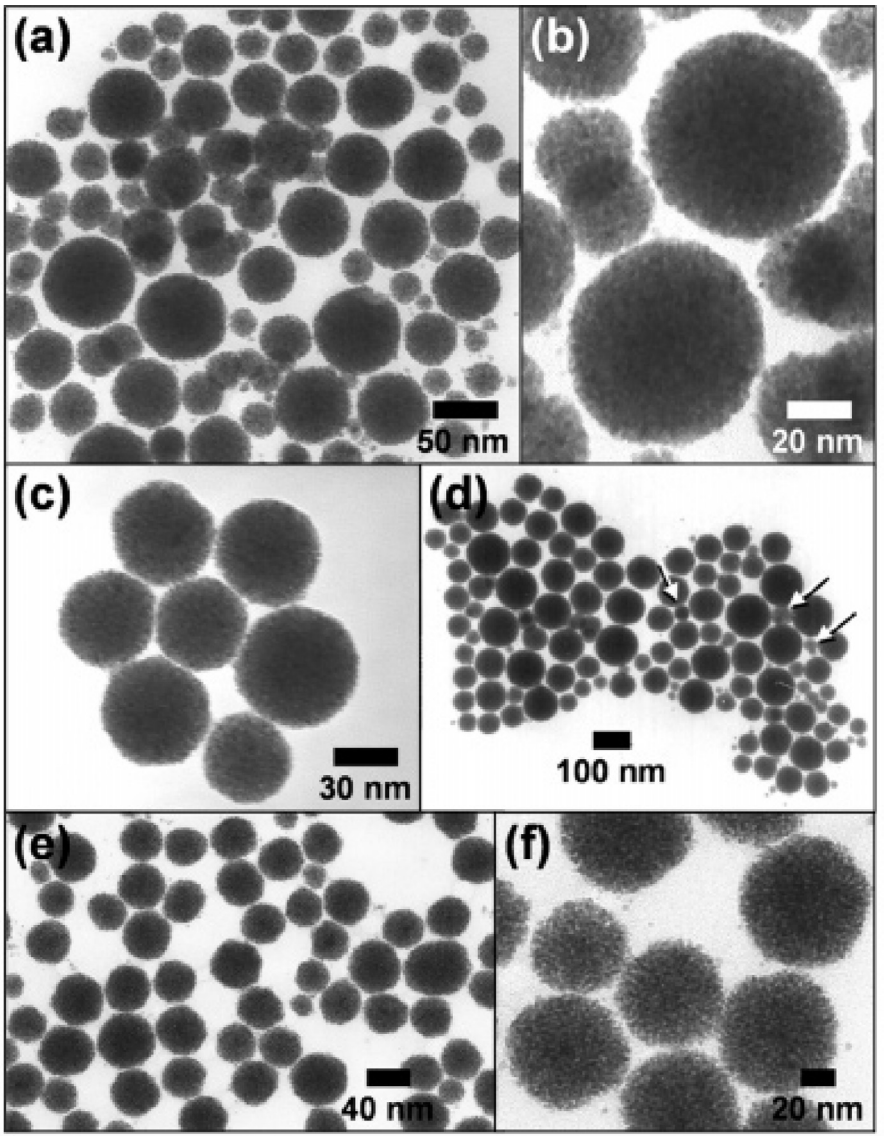

Fig. 9. TEM micrographs of spherical Rh nanoparticle aggregates synthesized using 920 mg of PVP (MW = 40 000) are shown in (a) and (b). Panel (c) shows a hexagonal superlattice, and panel (d) shows a superlattice formed after drying a suspension that was size-focused by centrifugation at 1 000 rpm. The arrows in (d) point to small spheres that sit in interstitial sites formed by larger spheres. A submonolayer of spherical aggregates deposited on a TEM grid and heated to 100 °C is shown in (e) and (f) (Adapted with permission from [75]. Copyright 2005, American Chemical Society).

In 2008, Somorjai et al. reported the synthesis of monodispersed sub-10 nm Rh nanocubes with high selectivity by a seedless polyol method [43]. In this approach, chemically adsorbed Br^- ions from tetradecyltrimethylammonium bromide (TTAB) could effectively stabilize the {100} faces of the Rh NPs and induce the evolution of nanocubes, as schematically shown in Fig. 11a. The TEM and HRTEM images in Fig. 11b reveal the formation of Rh nanocubes with high selectivity (>85%) and the Rh nanocubes are single crystalline.

https://doi.org/10.1016/j.heliyon.2019.e01165

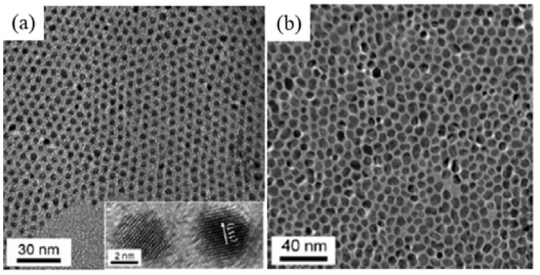

Fig. 10. Spherical Rh nanoparticles with average sizes of 4.8 ± 0.4 nm (a) and 7.1 ± 0.7 nm (b) prepared with the precursor concentration of 0.12 mmol and 0.24 mmol, respectively (Adapted with permission from [46]. Copyright 2007, Wiley-VCH).

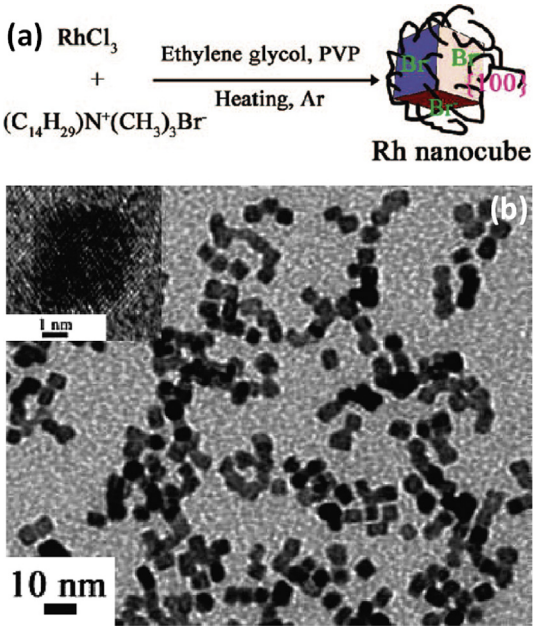

Fig. 11. (a) Schematic illustration showing the seedless polyol synthesis of Rh nanocubes, (b) TEM and HRTEM (inset) images of as-obtained Rh nanocubes (Adapted with permission from [43]. Copyright 2008, American Chemical Society).

Recently, Tanaka et al. studied the mechanism of formation of Rh nanocubes in the presence of tetradecyltrimethylammonium bromide (TTAB)and polyvinylpyrrolidone (PVP) in ethylene glycol by using in situ X-ray absorption fine structure (XAFS) technique in conjunction with other ex situ techniques [71]. As schematically shown in Fig. 12, they summarized four distinct stages for the formation of Rh NPs, including (i) exchange of the ligand for Rh^{3+} between Cl^{-} and Br^{-}, (ii) Rh_4 clusters act as the plausible nanoparticle nuclei, (iii) evolution of nuclei into Rh NPs, and (iv) transformation of irregularly shaped Rh NPs into cubic shape.

Schaak et al. demonstrated that proper selection of the polyol solvent can be used to manipulate the metal nanoparticle morphology [21]. Each polyol has a different

https://doi.org/10.1016/j.heliyon.2019.e01165

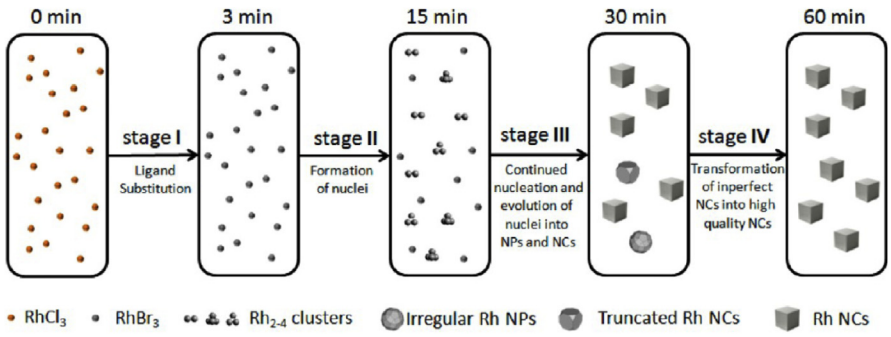

Fig. 12. Summary of the four-stage formation process of Rh NCs from $RhCl_3$: the Rh species shown in the five boxes represent the predominant but not the exclusive Rh species present, and the chemical transformations illustrated under each arrow represent the major characteristic, but not necessarily the only process involved during each stage (Adapted with permission from [71]. Copyright 2012, American Chemical Society).

oxidation potential which, along with the metal reagent, defines the temperature at which particle formation takes place. For a given system, particle growth will vary between a kinetic and thermodynamic regime depending on the thermal conditions, which can be modulated through selection of the appropriate solvent. Their strategy, which is demonstrated for the catalytically relevant Rh system, facilitates the high-yield synthesis of monodisperse Rh NPs with shapes that include icosahedra, cubes, triangular plates, and octahedra. Fig. 13 and Table 1 summarize the different results (size and shape) with diverse reaction conditions.

Nogami et al. reported the preparation of PVP-protected Rh NPs using $RhCl_3$ by a modified polyol method in ethylene glycol [74]. Through adjusting the concentration of $AgNO_3$, the morphologies of Rh NPs are changed. At a low $AgNO_3$ concentration, well-controlled cubic and octahedral Rh NPs with sizes of 7−14 nm could be easily obtained. The appearance of good control of morphology for Rh NPs is owing to their controlled growth of {100} and {111} selective surfaces, and the competitive growth between the two directions would lead to the formation of the morphology between cubic and octahedral shape (Fig. 14).

Son et al. found that Rh NPs with tetrahedral morphology show a 5.8- and 109-fold increase in activity for the hydrogenation of anthracene than spherical Rh NPs and commercial Rh/C catalyst, respectively [46]. The near-monodispersed tetrahedral Rh NPs preferentially exposing (111) planes were prepared by an organometallic approach, which used thermal decomposition of Rh complexes in oleylamine, followed by supporting on charcoal. These supported 4.9 ± 0.4 nm Rh nanotetrahedra and the mixture of tetrahedral and spherical Rh NPs obtained by changing conditions were showed in Fig. 15.

The Rh precursor in polyol method has a large influence on the shape and monodispersity of Rh NPs. Somorjai et al. synthesized monodispersed Rh NPs in the range of

https://doi.org/10.1016/j.heliyon.2019.e01165

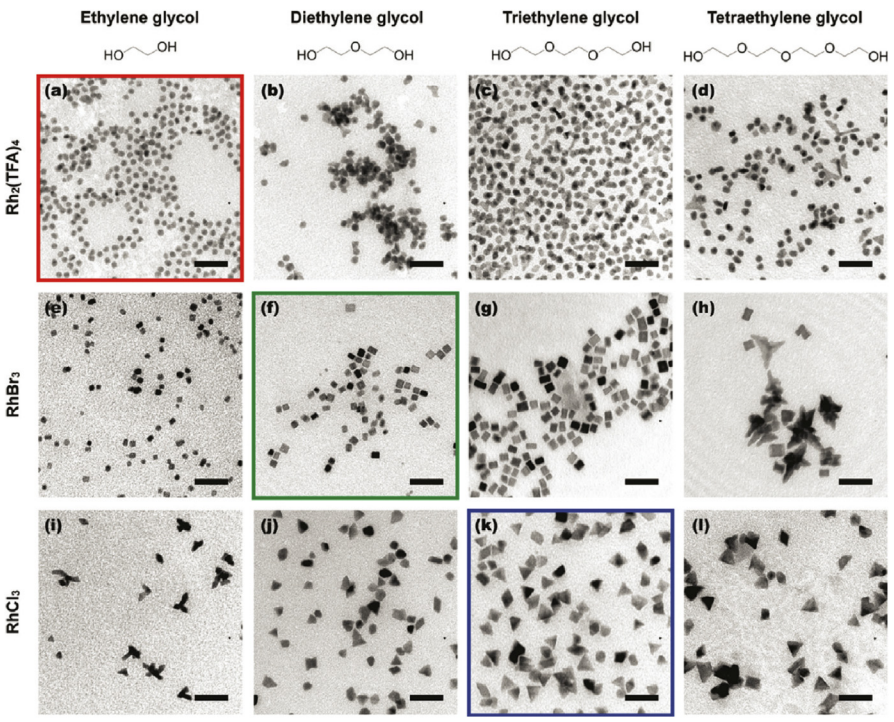

Fig. 13. Representative TEM images of Rh nanoparticles synthesized using ethylene glycol, diethylene glycol, triethylene glycol, and tetraethylene glycol solvents with the reagents (a−d) $Rh_2(TFA)_4$, (e−h) $RhBr_3$, and (i−l) $RhCl_3$ (TFA = trifluoroacetate). Outlined images indicate the set of reaction conditions which results in the most monodisperse yield of Rh icosahedra (red), cubes (green), and triangular plates (blue). Scale bars are 20 nm (Adapted with permission from [21]. Copyright 2011, American Chemical Society).

5−15 nm by a seedless polyol reduction in ethylene glycol, with PVP as a capping ligand [25]. They could regulate the proportion of various morphologies by changing the Rh precursor. In Fig. 16, the TEM measurements show that the Rh polygons are dominated by 40% hexagons, 14% pentagons ((111)-twinned decahedra), 25% triangles, 8% squares, and 12% irregular particles (9.8 ± 1.6 nm), which were synthesized at temperature at 185 °C for 2 h, and using 2.5 mM $[Rh(Ac)_2]_2$ as Rh precursors.

Decahedral nanoparticles have received great attention owing to their unique symmetry and strain-energy distribution. However, it is more difficult to synthesize decahedral Rh NPs compared with other noble metals. Not long ago, Xia et al. [73] reported the facile synthesis of Rh decahedral NPs in high purity, with sub-20 nm sizes using a robust, one-pot method based on polyol reduction [73], as shown in Fig. 17 for the TEM and HRTEM images. They have further studied that the relationship between the yield of Rh decahedral NPs and reduction conditions, including the concentration of $Rh(acac)_3$, the molecular weight and amount of PVP, and chain length of the polyol.

https://doi.org/10.1016/j.heliyon.2019.e01165

Table 1. Summary of reaction conditions and results (Adapted with permission from [21]. Copyright 2011, American Chemical Society).

Image number in Fig. 13	Precursor	Polyol solvent	Approx nucleation temp (°C)	Set focusing temp (°C)	Predominant (>25%) morphologies
a	$Rh_2(TFA)_4$	EG[a]	105−110	160	Icosahedron
b	$Rh_2(TFA)_4$	DEG[b]	120−130	170	Icosahedron
c	$Rh_2(TFA)_4$	TREG[c]	130−140	180	Icosahedron, 3-fold branched
d	$Rh_2(TFA)_4$	TEG[d]	135−145	185	Icosahedron, mixed anisotropic
e	$RhBr_3$	EG	80−90	120	Truncated cube
f	$RhBr_3$	DEG	105−110	140	Cube
g	$RhBr_3$	TREG	110−120	145	Cube, bar
h	$RhBr_3$	TEG	115−125	150	Concave cube, mixed concave, branched
i	$RhBr_3$	EG	70−80	115	3-fold branched, triangular plate
j	$RhBr_3$	DEG	85−95	130	Triangular plate, spherical polyhedron
k	$RhBr_3$	TREG	95−105	140	Triangular plate
l	$RhBr_3$	TEG	100−110	145	Triangular plate, octhedron

[a] EG = ethylene glycol.
[b] DEG = diethylene glycol.
[c] TREG = triethylene glycol.
[d] TEG = tetraethylene glycol.

Through varying the denticity of the ligand coordinating to Rh in the precursors and varying the molecular weight of PVP, Xia et al. demonstrated a facile protocol for the synthesis of Rh icosahedra with average sizes up to 12.0 ± 0.8 nm by using $Rh(acac)_3$ as a precursor and PVP as a reducing agent and a colloidal stabilizer in benzyl alcohol [41]. With this method, the reduction kinetics can be manipulated to promote the formation of twin defects in the Rh NPs (Fig. 18). When $Rh(acac)_3$ is replaced by other precursors containing mono-dentate ligands, single-crystal Rh NPs are obtained due to the acceleration of reduction rate. By increasing the molecular weight of PVP from 10 000 to 1 300 000, the resulting Rh NPs are transformed from single-crystal octahedra to multiply twinned icosahedra and stacking-fault-lined plates. These results suggest that the successful preparation of Rh icosahedra could be facilitated by varying the binding strength of a ligand to Rh in the precursor and/or the molecular weight of PVP to optimize the reduction kinetics.

To overcome the extremely high specific surface free energy of Rh NPs, Sun et al. have developed an electrochemical square-wave-potential (SWP) approach to the generation of convex NMNPs with high-index facets, and they extended this method to the successful synthesis of tetrahexahedral (THH) Rh NPs enclosed by {830} high-index facets attributed to the dynamic oxygen adsorption/desorption process [47]. Fig. 19 shows the morphological and structural characterizations of the Rh THH nanocrystals obtained by SWP method. The average value of angle on the projection

https://doi.org/10.1016/j.heliyon.2019.e01165

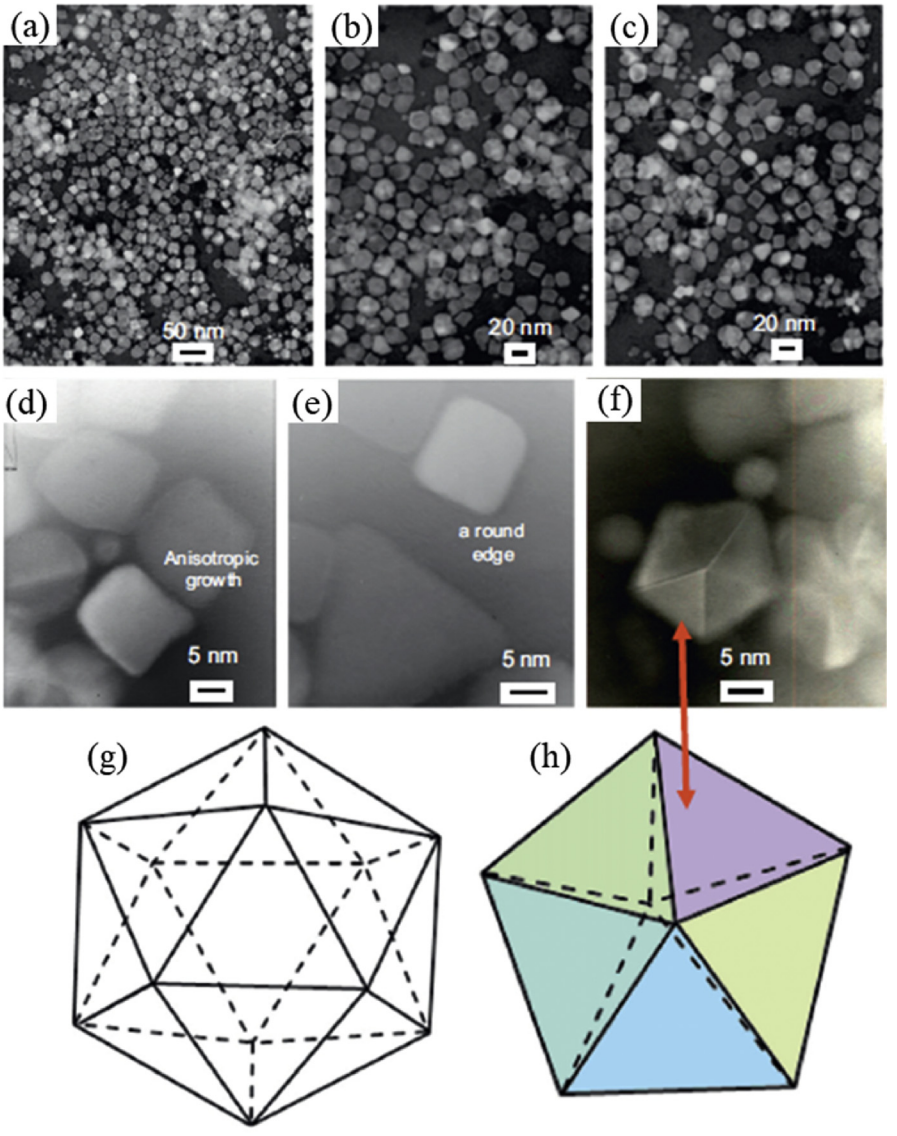

Fig. 14. (a–c) Rh NPs of various sizes and shapes, including cubic, octahedral, and porous Rh NPs (with the addition of 0.002 M $AgNO_3$ synthesized by a polyol method in EG at 160 °C, the reduction time for $RhCl_3$ of ~20 min), (d–f) individual particles with different morphologies, (g, h) models of multiply twinned icosahedron and decahedron (Adapted with permission from [74]. Copyright 2011, Elsevier B. V.).

of the THH Rh NC was measured in Fig. 19c, and it was quite close to the theoretical values on a THH NC enclosed by {830} facets, which are periodically composed of two {310} subfacets followed by a {210} subfacet, as illustrated in Fig. 19e.

2.3.3. Synthetic approaches for Rh nanoplates or nanosheets

Due to their face-centered cubic (fcc) phase, the shape-controlled synthesis of Rh NPs has focused on the isotropic structure. However, anisotropic Rh NPs such as

https://doi.org/10.1016/j.heliyon.2019.e01165

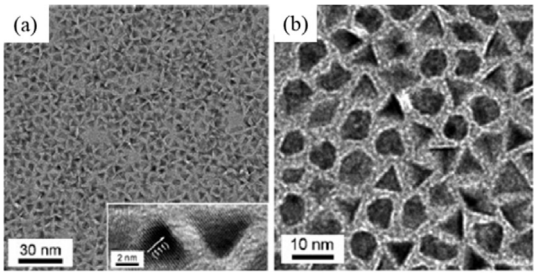

Fig. 15. (a) Low-magnification TEM and HRTEM images (insets) of 4.9 ± 0.4 nm tetrahedral, (b) TEM images of the mixture of tetrahedral and spherical Rh nanoparticles (Adapted with permission from [46]. Copyright 2007, Wiley-VCH).

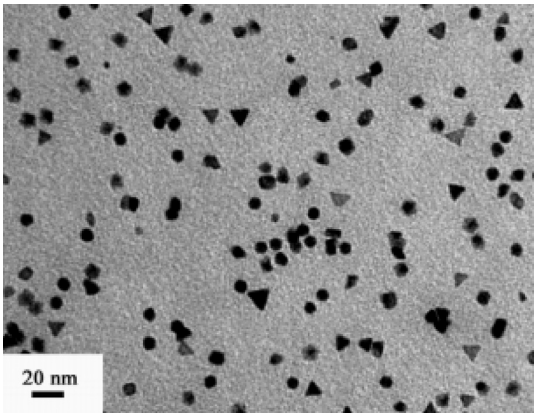

Fig. 16. Low-magnification TEM images of as-obtained Rh NPs synthesized in 20 mL of ethylene glycol under an Ar atmosphere (2.5 mM $[Rh(Ac)_2]_2$, 100 mM PVP, 185 °C, 2 h, 9.8 ± 1.6 nm) (Adapted with permission from [25]. Copyright 2010, American Chemical Society).

2D nanoplates or nanosheets enclosed mainly by {111} facets have also been synthesized with the assistance of a capping agent. Schaak et al. found that Rh nanoplates could be prepared in the as-obtained particles by changing the experimental conditions [21]. As shown in Fig. 13i–l and Table 1, triangular Rh nanoplates have been made using $RhCl_3$ in the polyol solvents (EG, DEG, TREG, TEG) at different temperature intervals. It is obviously that $RhCl_3$ tend to produce branched particles in EG, but with larger polyols, the products are predominantly triangular plates.

Son et al. reported the successful synthesis of unprecedented ultrathin Rh nanoplates through kinetically controlled growth at low temperature by using oleylamine as a coordinating and capping agent [78]. Fig. 20 shows the two view of plates varied from triangle to qudrangle (trapezoid, rhombus). The triangular nanoplates are observed as major shape and the prepared Rh nanoplates are ultrathin with an average thickness of only 1.3 ± 0.2 nm. They suggested a plausible mechanism formation for the growth of Rh nanoplates under the assistance of oleylamine on the basis of the chains *via* van der Waals interaction between alkyl groups to form lamellar structure (Fig. 20c).

https://doi.org/10.1016/j.heliyon.2019.e01165

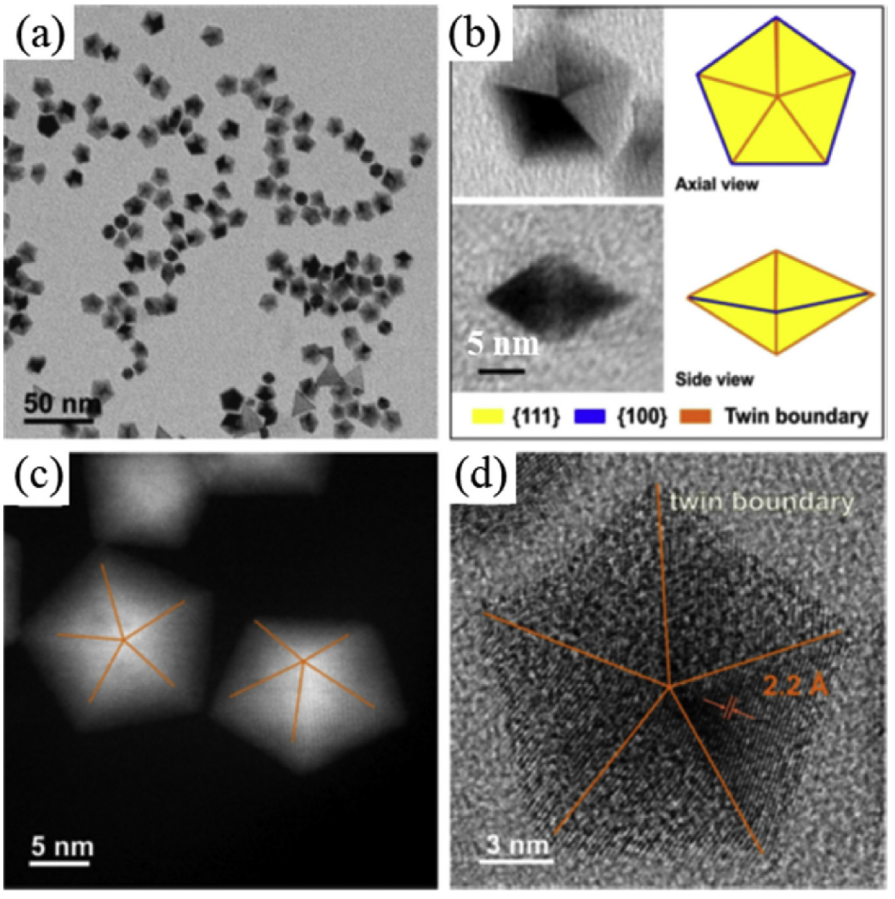

Fig. 17. (a) TEM image of Rh decahedra prepared using the standard procedure, (b) TEM images and schematic models of a decahedron in two different orientations (axial and side view), (c) HAADF-STEM image of the Rh decahedra, (d) High-resolution TEM image taken from an individual particle in sample (a) where the twin defects are marked with orange lines (Adapted with permission from [73]. Copyright 2018, Wiley-VCH).

In 2014, Li et al. reported the fabrication of PVP-supported Rh ultrathin nanosheets using a facile solvothermal method with a thickness of only one layer and the yield of 100 % [79], as shown by Fig. 21 for their microscopic characterizations. Various characteristic means have proved that the Rh nanosheets are composed of planar single-atom-layered sheets and the thickness of a Rh nanosheet is <4 Å. Furthermore, they carried out density functional theory (DFT) studies to illustrate that the single-layered Rh nanosheet involves a δ-bonding framework, which stabilizes the single-layered structure together with the PVP ligands.

2.3.4. Synthetic approaches for branched or dendritic Rh NPs

In addition to the more commonly spherical and cubic morphologies, Rh NPs can also be made into branched or dendritic shapes. Wang et al. studied the shape-dependent electrochemical properties of Rh nanostructures prepared by tunable

https://doi.org/10.1016/j.heliyon.2019.e01165

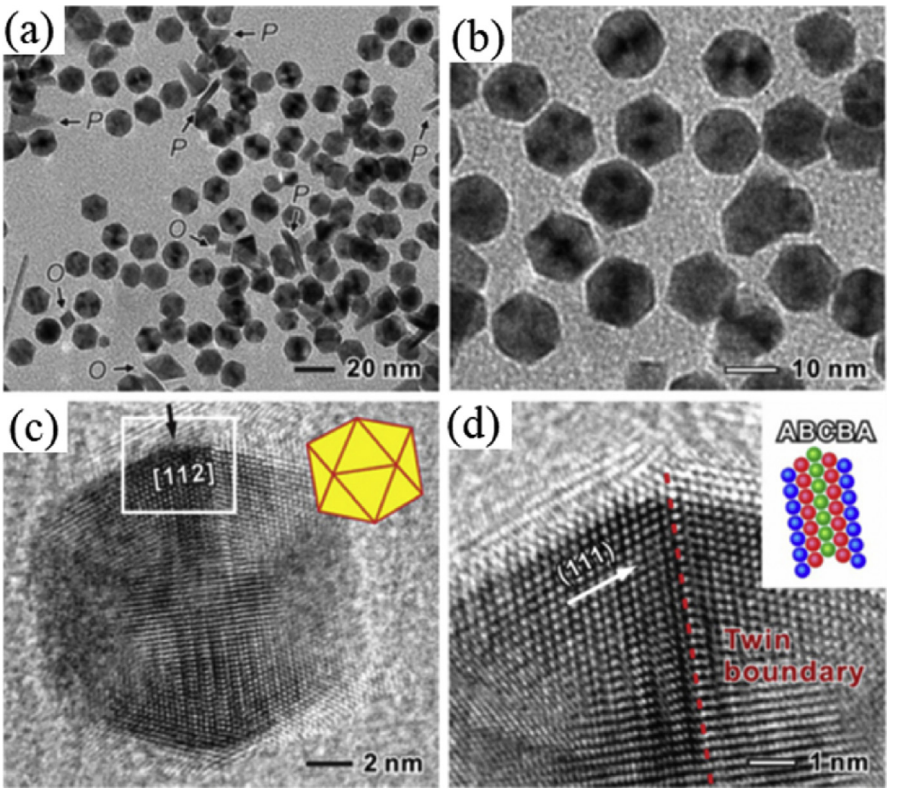

Fig. 18. (a,b) TEM images of Rh icosahedra with an average diameter of 12.0 ± 0.8 nm, which were synthesized by reducing $Rh(acac)_3$ in benzyl alcohol containing PVP as a stabilizer and a reducing agent (In a, Rh plates and octahedra are indicated by P and O, respectively), (c) HRTEM images of an individual icosahedron, (d) atomic resolution TEM image taken from the edge marked by a box in c, revealing the twin boundary on the icosahedron (Adapted with permission from [41]. Copyright 2016, Wiley-VCH).

aqueous phase synthesis [76]. The highly selective one-pot synthetic method for Rh NPs they used have been achieved different morphologies such as horned particles, cubes, dendrites, and networks through the synergetic effect of sodium lauryl sulfate (SLS) and halogen anions (F^-, Cl^-, Br^-, I^-). The dendritic structure of Rh NPs was first synthesized, and their morphology was shown in Fig. 22.

The zerovalent species, including atoms, clusters, and nanocrystallites, can all be oxidized back to their ionic form, and thus can alter the crystallinity, size, shape, morphology, and growth kinetics of products. To capitalize on that, oxidative etching is used for the synthesis of metal nanoparticles. For example, when coupling the O_2 from air with a coordination ligand, especially a halide such as Cl^-, Br^-, or I^-, they can serve as an effective etchant in a solution-phase synthesis [80]. The etching prefers to selectively start from the defect sites rather than a region with perfect crystallinity, thus the synthesis of Rh NPs in use of a salt precursor containing Cl^- tends to form a single-crystal structure [42, 43, 44]. As a result, to obtain Rh twinned nanocrystals, any salt precursor that contains halide should not be used to

https://doi.org/10.1016/j.heliyon.2019.e01165

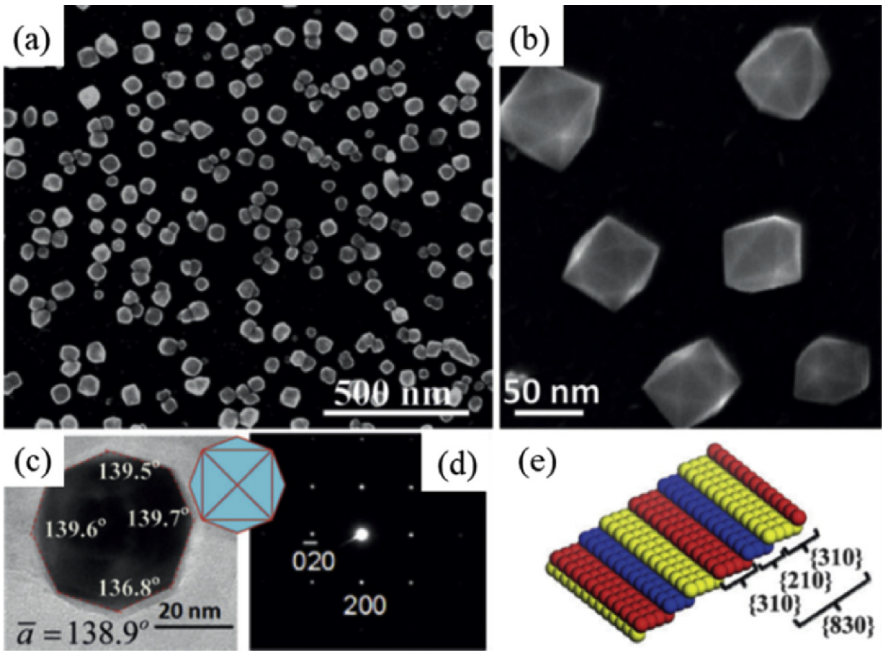

Fig. 19. (a) Low- and (b) high-magnification SEM images of THH Rh NPs obtained at E_U of 0.70 V and E_L of −0.07 V, (c) TEM image and (d) SAED pattern of a THH Rh nanoparticle along the [001] direction, (e) atomic arranged model of {830} plane (Adapted with permission from [47]. Copyright 2014, Wiley-VCH).

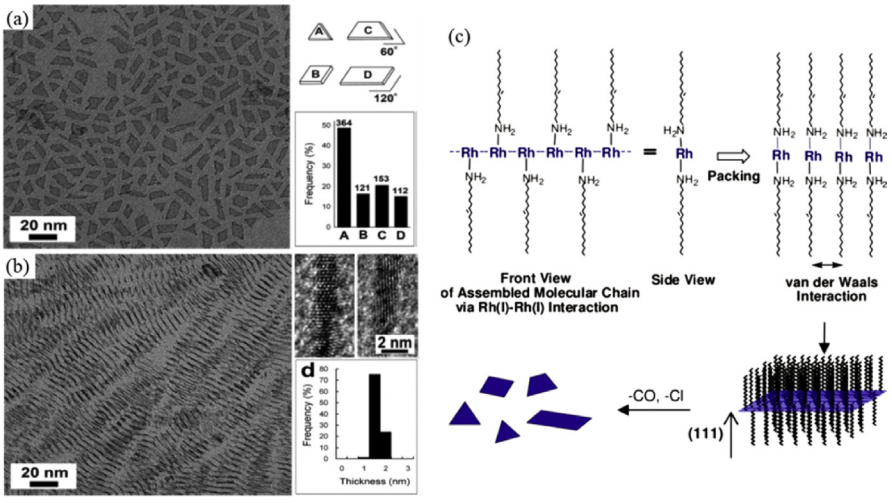

Fig. 20. (a) TEM image and shape distribution diagram by investigating 750 plates, (b) TEM and HRTEM images of the cross-sectional view and their thickness distribution diagram of the obtained rhodium nanoplates, (c) suggested growth mechanism of Rh nanoplates (Adapted with permission from [78]. Copyright 2010, American Chemical Society).

completely eliminate the etching process. Xia et al. demonstrated a facile polyol approach to the synthesis of starfish-like Rh NPs with the use of a halide-free precursor $[Rh(CF_3COO)_2]_2$ by replacing the conventional precursor containing Cl^- [77]. Successfully, they prepared the starfish-like Rh NPs with a five-fold twinned

https://doi.org/10.1016/j.heliyon.2019.e01165

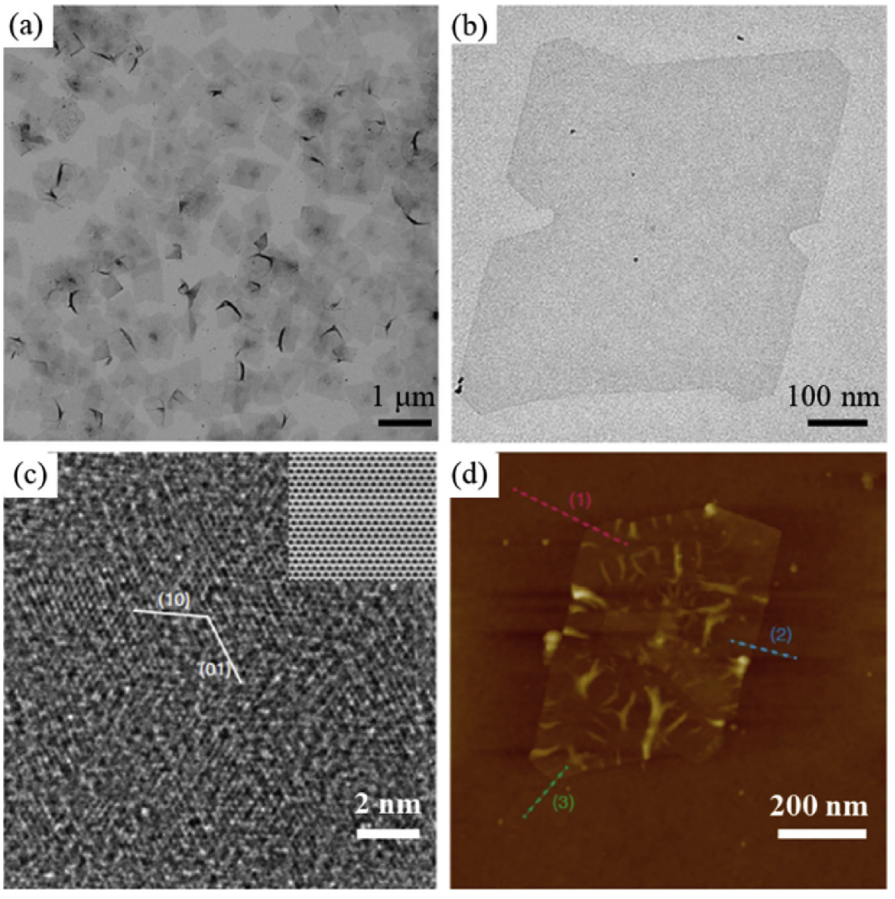

Fig. 21. (a) Low-magnification TEM image of the PVP-capped Rh nanosheets, (b) High-magnification TEM image of the PVP-capped Rh nanosheet, (c) Aberration-corrected microscopy image of a PVP-capped Rh nanosheet (inset, the corresponding filtered image using the crystallographic average method to improve signal-to-noise ratio), (d) AFM image and the corresponding height profiles of a bare Rh nanosheet (Adapted with permission from [79]. Copyright 2014, Nature Publishing Group).

structure of high yield (Fig. 23). Under thermodynamically controlled conditions, the starfish-like Rh NPs are evolved from initial decahedral Rh particles; the process is driven by Ostwald ripening through producing arms from the five corners of the decahedral nanoparticles gradually.

Recently, Yang et al. reported the synthesis of dendritic Rh NPs with an overall size of 24.4 nm (Fig. 24a and b) by directly reducing $Rh(acac)_3$ in oleylamine at elevated temperature [81]. In a typical synthesis, 0.5 mmol of $Rh(acac)_3$ was added to 20 mL of oleylamine in a three-necked flask equipped with a condenser and a stir bar. The solution was brought to and kept at 160 °C for 2 h under flowing N_2 for the reduction of Rh precursor by oleylamine. After reaction, the dendritic Rh NPs were purified by precipitation with methanol, centrifugation, washing with methanol, and re-dispersed in 20 mL of toluene. Oleylamine is a common reducing agent for the synthesis of NMNPs [82, 83, 84, 85, 86]. Through FI-IR and ^1H NMR (nuclear magnetic resonance

https://doi.org/10.1016/j.heliyon.2019.e01165

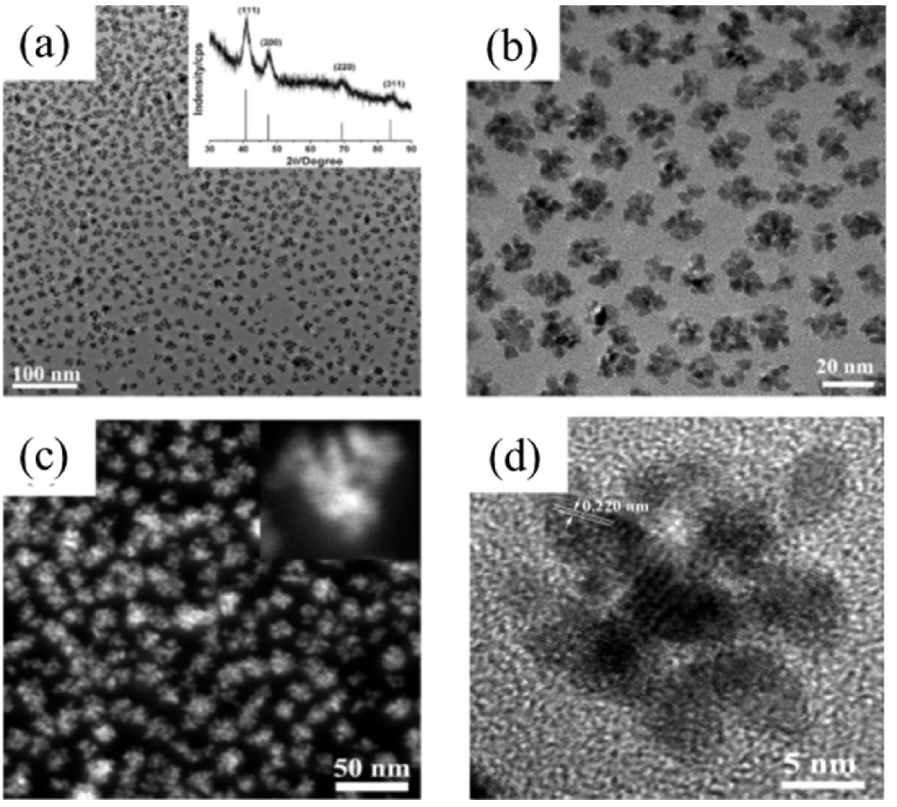

Fig. 22. Representative TEM and HRTEM (a, b, d) images of Rh nanodendrites synthesized at 220 °C for 6 h, the high-angle annular dark field (HAADF)-STEM image (c), and XRD profile of as-synthesized products (a, inset) (Adapted with permission from [76]. Copyright 2010, American Chemical Society).

spectroscopy) analyses, Liu *et al.* elucidated the mechanism for the NMNPs formed by oleylamine reduction [87]. In brief, amine ligands are firstly oxidized to amides during the reduction of metal precursors, and then form a protecting layer of hydrogen bond network on the surface of NMNPs. Therefore, the mechanism for producing Rh nanodendrites in oleylamine could be depicted by the scheme in Fig. 24c [81]. At initial stage, the $Rh(acac)_3$ are reduced into Rh atoms by oleylamine, which grow into Rh particles, while oleylamides are simultaneously formed from oleylamine as the capping agent to stabilize the Rh particles. Then the particle aggregation would compete with the oleylamide passivation, resulting in the formation of a large number of Rh particle aggregates in the solution (step (i) in Fig. 24c). Finally, the Rh particle aggregates continuously grow with the expense of small particles in solution *via* a ripening process to form larger and more stable dendritic Rh NPs (step (ii) and (iii) in Fig. 24c).

2.3.5. Synthetic approaches for Rh NPs with concave or frame structures

Maneuvering the shape to control their facets and curvature of NMNPs has been considered as a powerful means for tailoring their properties and enhancing their

https://doi.org/10.1016/j.heliyon.2019.e01165

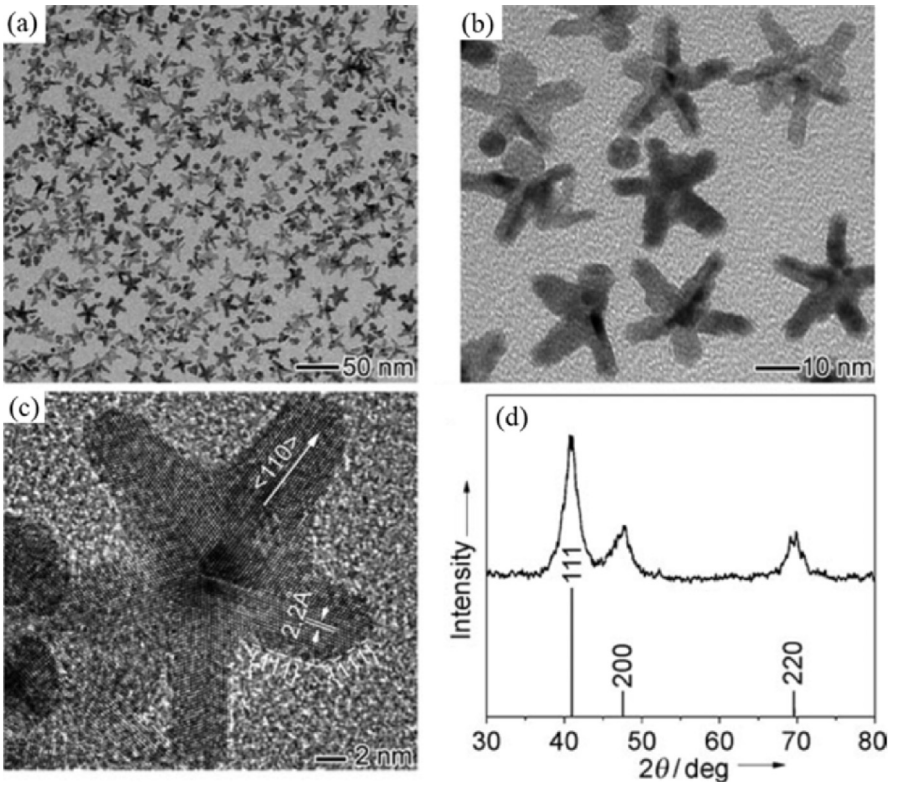

Fig. 23. (a, b) TEM images, (c) HRTEM image, and (d) XRD pattern of a typical sample of starfish-like Rh NPs prepared using polyol reduction at 180 °C for 6 h (Adapted with permission from [77]. Copyright 2010, Wiley-VCH).

performance. In recent years, many studies have found that NMNPs under kinetically controlled conditions could break the thermodynamic confinement to form particles with concave surfaces [88, 89]. Take advantage of this strategy, Rh NPs with concave or frame structures can be specifically synthesized in the presence of a capping agent and at an appropriate reduction rate.

Xia et al. demonstrated a simple and versatile polyol process for the synthesis of Rh concave nanocubes by manipulating the reaction kinetics [72]. By injecting the precursor at a slow rate of 4 mL h^{-1} into a growth solution using a syringe pump, Rh concave nanocubes of 15 nm in edge length with a cubic symmetry were deterministically obtained in a high yield approaching 100%. Fig. 25 shows the morphological and structural characterizations of Rh concave nanocubes, indicating the concave surfaces on the six side faces of each Rh nanoparticle and the surfaces are bounded by a mix of both {100} and {110} facets, where the presence of a high fraction of {110} facets on the surface is attractive for applications in catalysis. This strategy has also been extended to the syntheses of Rh-based bimetallic nanoparticles with concave surfaces.

https://doi.org/10.1016/j.heliyon.2019.e01165

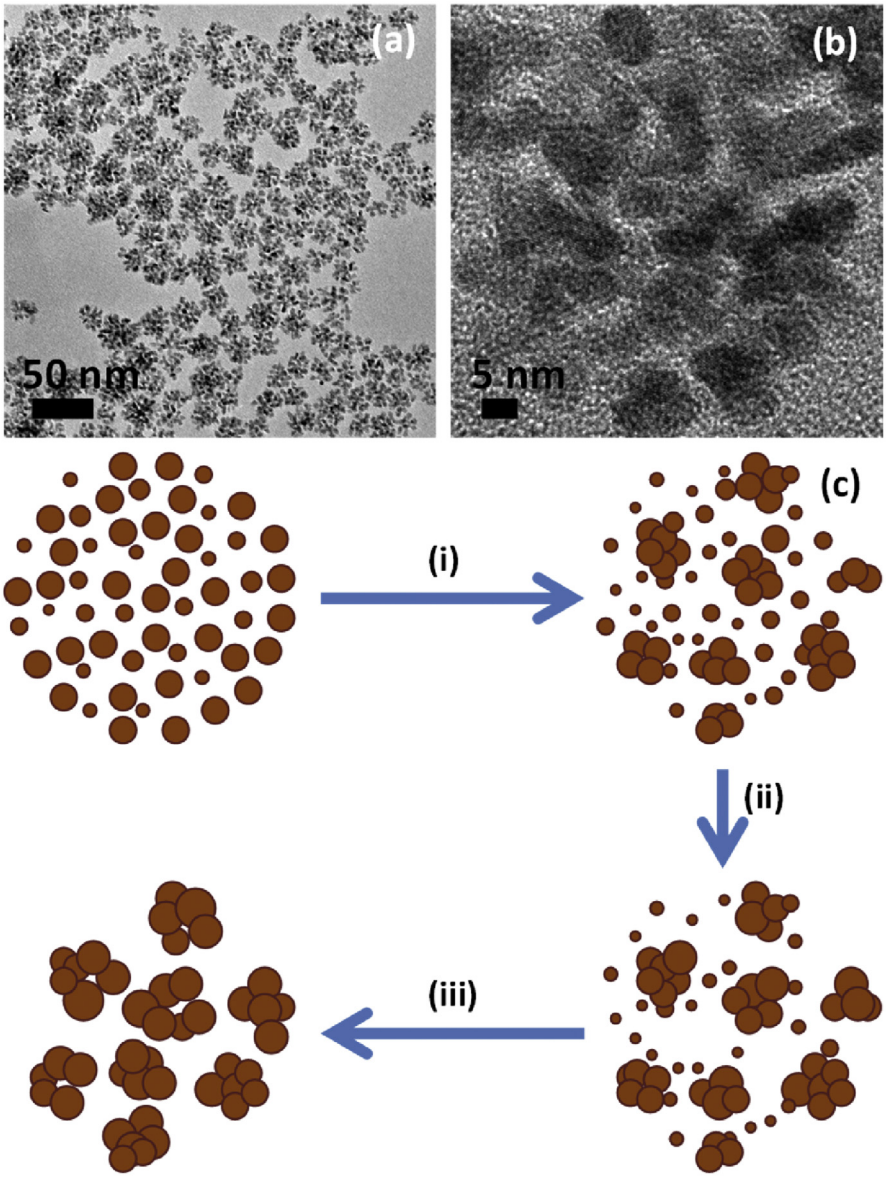

Fig. 24. (a) TEM image and (b) HRTEM image of the dendritic Rh NPs synthesized in oleylamine at temperature of 160 °C; (c) Schematic illustration showing the mechanism for forming dendritic Rh NPs *via* the reduction of $Rh(acac)_3$ in oleylamine at elevated temperature: (i) competition between particle aggregation and oleylamide passivation results in the formation of particle aggregates; (ii, iii) particle aggregates grow into nanodendrites *via* a ripening process (Adapted with permission from [81]. Copyright 2014, Royal Society of Chemistry).

In 2012, Xia et al. used this strategy to complete the synthesis of Pd-Rh bimetallic core−frame concave nanocubes and Rh cubic nanoframes by confined overgrowth of Rh atoms at the corners and edges of Pd cubic seeds [48]. Fig. 26 shows the morphology and a summary of all the major steps. The three steps involve (i) selective nucleation of Rh at the corners and edges of the Pd nanocubes, (ii) the formation

https://doi.org/10.1016/j.heliyon.2019.e01165

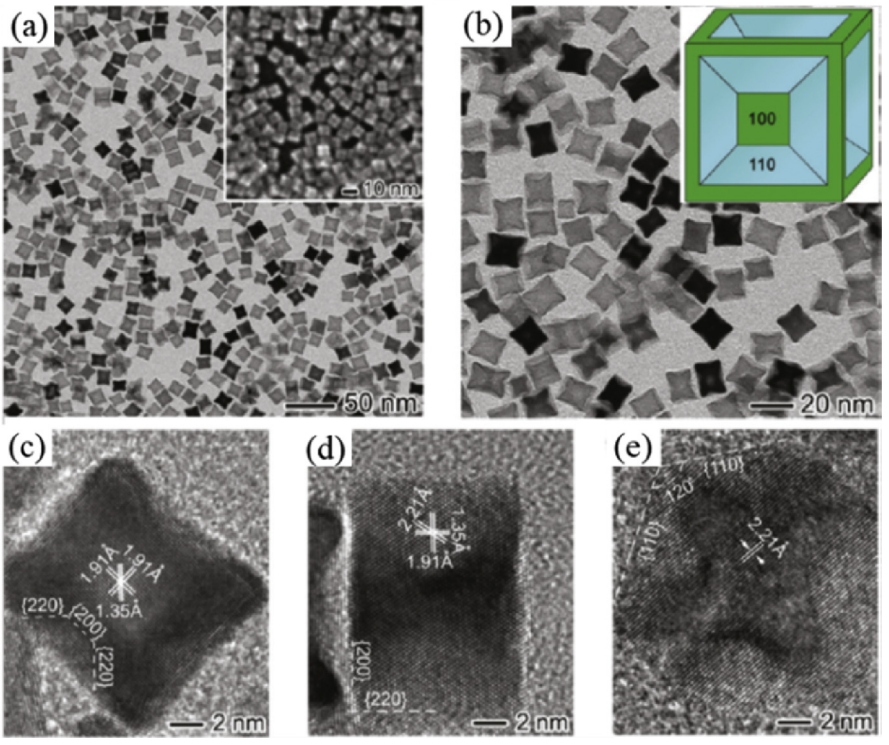

Fig. 25. Morphological and structural characterizations of a typical sample of Rh concave nanocubes prepared at 140 °C with an injection rate of 4 mL h^{-1}, (a, b) TEM images of the as-prepared sample, (c−e) HRTEM images of individual concave nanocubes recorded along the [100, 110,111] zone axes; the insets in a and b show a typical SEM image of the concave nanocubes and the 3D model, respectively (Adapted with permission from [72]. Copyright 2011, American Chemical Society).

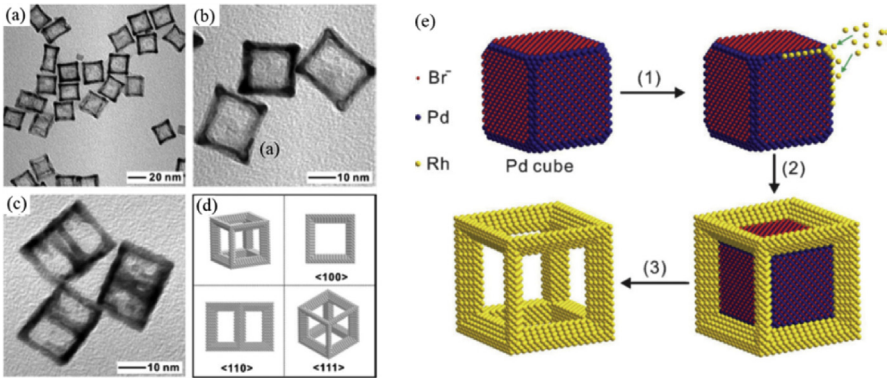

Fig. 26. (a) TEM images of Rh cubic nanoframes obtained by selectively etching away the Pd cores from the Pd-Rh core−frame nanocubes; (b, c) TEM images of Rh cubic nanoframes projected along <100> and <110> zone axes, respectively; (d) drawings that present a 3D model of the Rh cubic nanoframe and its projections along <100>, <110>, and <111> zone axes, (e) the three major steps involved in the synthesis of Pd-Rh core−frame nanocubes with concave faces and Rh cubic nanoframes (Adapted with permission from [48]. Copyright 2012, Wiley-VCH).

https://doi.org/10.1016/j.heliyon.2019.e01165

of Pd-Rh bimetallic concave nanocubes and their subsequent conversion into Rh cubic nanoframes, and (iii) the formation of Rh cubic nanoframes by selectively etching away the Pd cores (Fig. 26e).

Further, Xia et al. reported a facile formation of Rh tetrahedrons with concave surfaces by interplaying reaction kinetics, facet-selective capping, and surface diffusion of atoms [90]. The uniform Rh concave tetrahedrons were demonstrated to be encased by a mix of {111} and {110} facets, and they could only be formed under a moderate reduction rate for the Rh^{3+} precursors to make sure of the coordination with a proper polyol. Rh tetrapods were generated by Rh atoms, which were spontaneously nucleated and subsequently selectively deposited onto the corner sites.

Guo et al. reported a simple and effective site-selective etching strategy to control the concavity of Rh nanocubes enclosed by high-index facets by using hydrochloric acid as an etchant [91]. In Fig. 27, the thorough structural characterization of Rh concave nanocubes was carried out along three typical zone axes [100, 110,111] of face-centered cubic (fcc) nanocubes. Three different zone axes of the nanoparticles could explicitly identify the structure of the concave nanocubes. Though manipulating the degrees of concavity or Miller indices of high-index facets is significant for metal nanoparticles to further tailor their properties, generating a concave surface with negative curvature is still in the early development stage and tuning the degree of concavity remains a challenge.

2.3.6. Synthetic approaches for Rh NPs with other morphologies

Apart from the shapes mentioned above, there are also a number of Rh NCs with other morphologies, e.g. wires, chains, and tubes.

Lu et al. successfully synthesized hollow Rh nanotubes with uniform structures through the galvanic replacement reaction between Ag nanowires and aqueous $RhCl_3$ in saturated NaI solutions at room temperature [92]. The approach was effective because I^- anions could reduce the redox potential of Ag species and dissolve the formed AgI precipitates.

Schaak et al. prepared magnetically separable hydrogenation nanowire catalysts decorated by Rh NPs [49]. Fig. 28 shows the TEM image of Rh nanowires templated by wild-type (WT) M13 bacteriophage, on which the Rh NPs are each ~5 nm in diameter. The nanowires could only form under conditions where a cationic metal reagent is used. The formation of nanowires might be the result of cationic metal complexes adsorbing nonspecifically along the anionic surface and remaining stable even after reduction and nucleation of the nanoparticles.

For most catalytic reactions, the shape of the catalysts is closely related to the activity and selectivity. Different morphologies may have different catalytic performances in

https://doi.org/10.1016/j.heliyon.2019.e01165

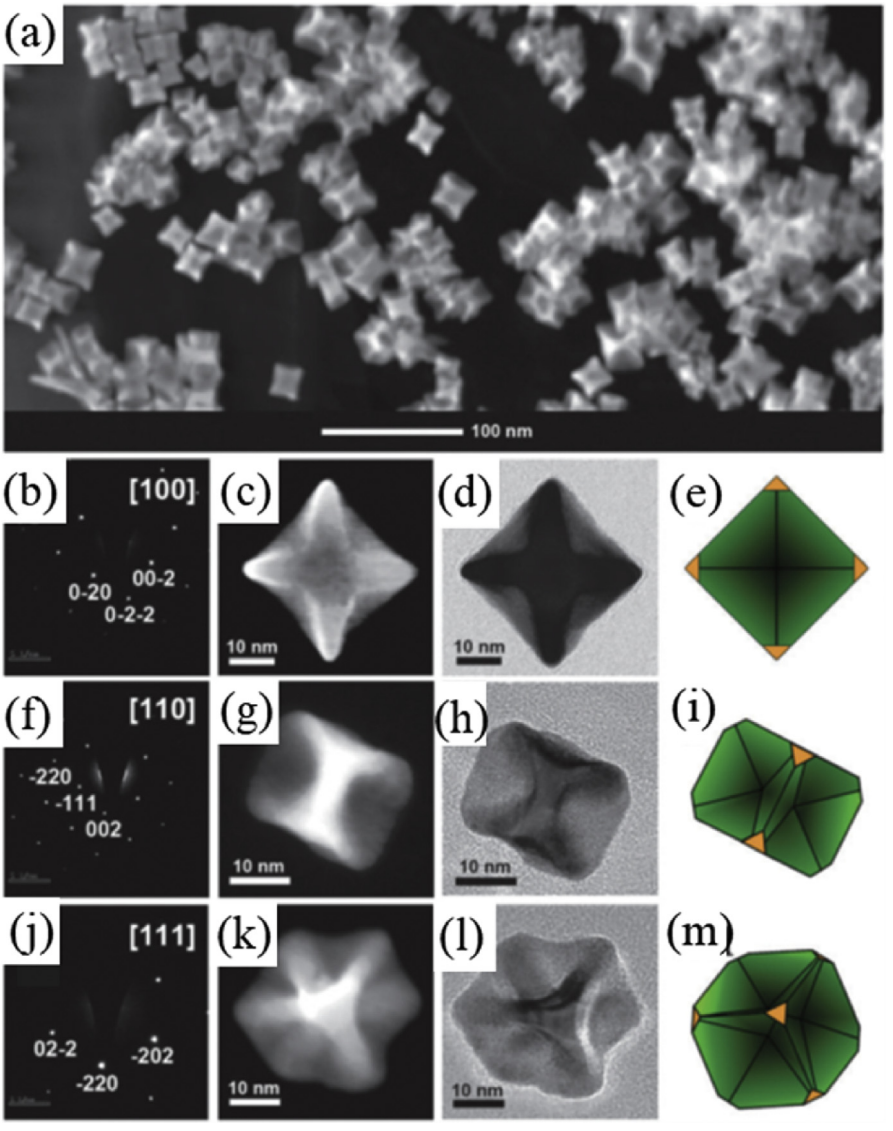

Fig. 27. (a) Large-area STEM image of Rh concave nanocubes. (b, f, j) SAED patterns, (c, g, k) STEM images, (d, h, l) TEM images and (e, i, m) schematic geometric models of individual concave nanocubes oriented along the [100] (b−e), [110] (f−i), and [111] (j−m) zone axes (Adapted with permission from [91]. Copyright 2014, Royal Society of Chemistry).

various reactions. From the perspective of preparation conditions, morphological control can be achieved in many ways, including those based on the use of surface capping agents, manipulation of reduction kinetics, control of surface diffusion rate, management of oxidation etching, and electrochemical alteration [42].

2.4. Applications of Rh NPs with different sizes/morphologies

Similar to other noble metals, Rh NPs have excellent catalytic properties for many catalytic reactions, including CO oxidation, hydrogenation, hydroformylation, and

https://doi.org/10.1016/j.heliyon.2019.e01165

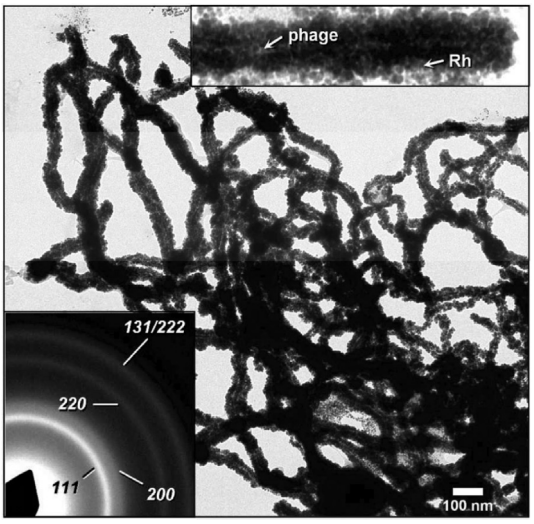

Fig. 28. TEM images of WT phage coated with Rh nanoparticles using $RhCl_3$ as the metal salt reagent and SAED pattern confirming the presence of fcc Rh (Adapted with permission from [49]. Copyright 2009, American Chemical Society).

various electrochemical oxidation reactions [93, 94, 95, 96, 97, 98, 99, 100, 101, 102, 103]. However, the relationship between the catalytic properties of Rh NPs and their size/shape has only been studied in recent years. Herein, several typical examples will be exhibited to highlight the catalytic activity/selectivity enhanced by size- and shape-controlled synthesis for facilitating the use of Rh NPs in catalytic applications.

2.4.1. Catalytic applications of size-controlled Rh NPs

As depicted in previous sections, the size control of Rh NPs is significant for many catalytic reactions. Table 2 summarizes the size effect of Rh-based catalysts on the catalytic reactions that have been reported in literatures.

In recent years, there have been many studies on the size-regulated Rh NPs used to enhance catalytic performance of hydrogenation [62, 63, 104, 110, 111, 112]. Somorjai et al. synthesized size-tunable monodispersed Rh NPs in a range of 5−15 nm by a one-step polyol reduction and studied their unique properties for a heterogeneous catalytic reaction (hydrogenation) [113]. Using $Rh(acac)_3$ as the metal precursors, they demonstrated the well-controlled polyol reduction kinetics for tuning the size of the Rh NPs by changing the $Rh(acac)_3$ concentration in a proper range. Monolayer films were produced for the differently sized Rh NPs on silicon wafers by Langmuir-Blodgett method. Through catalytic tests, they revealed that the Rh particle monolayers as model heterogeneous catalysts are active for ethylene hydrogenation.

A size-dependent effect was also observed for CO oxidation using supported Rh NPs [22, 106, 114]. Hensen et al. reported the preparation of Rh NPs on several oxide

https://doi.org/10.1016/j.heliyon.2019.e01165

Table 2. Typical Examples showing the effect of Rh nanoparticle size on various catalytic reactions.

Size range (nm)	Stabilizer/support	Precursor	Reaction type	Ref.
2.3−7.8	MWNTs[a]	$RhCl_3$	Hydrogenation	[104]
0.96−1.65	Quinine/Al_2O_3	$Rh(acac)_3$	Hydrogenation	[63]
2−8	PVP/γ-Al_2O_3	$RhCl_3 \cdot xH_2O$	Sonogashira coupling	[105]
2−11	PVP	$Rh(acac)_3$	CO oxidation	[22]
1.6−8	$CeZrO_2$, ZrO_2,SiO_2	$Rh(NO_3)_3 \cdot nH_2O$	CO oxidation	[106]
1−9	ZrO_2, CeO_2,SiO_2, $CeZrO_2$	$Rh(NO_3)_3 \cdot nH_2O$	steam methane reforming	[107]
<1.5−6	SiO_2	$RhCl_3$, $[Rh(COD)Cl]_2$	Hydroformylation	[108]
0.7−6	ZrO_2	$RhCl_3 \cdot xH_2O$	Ethane hydrogenolysis	[109]
2−6	HEA16BF_4	$RhCl_3$	Hydrogenation	[110]
0.5−3.5	HEA16HCO_3	$RhCl_3$		
5−10	[BMIm][PF_6]	$Rh(OAc)_3$, $Rh(acac)_3$	Hydrogenation	[62]
1.6−4	–	$Rh(\eta^3\text{-}C_3H_5)_3$	Hydrogenation	[69]

[a] MWNTs = multiwalled carbon nanotubes.

supports ($CeZrO_2$, ZrO_2,SiO_2) by incipient wetness impregnation [106]. The particle size (d_{Rh}) of the reduced catalysts is within the range 1.6 nm−8 nm. In applications, Rh NPs stabilized by reducible supports with very small size are completely oxidized under CO oxidation conditions, whereas particles larger than 4 nm maintain their metallic state. This can represent that smaller Rh NPs are more catalytically active. Their study came up with the result that the supports could affect not only stability but also the oxidation behavior of the Rh NPs and therefore the catalytic activity. More remarkably, they found the Rh NPs supported on ceria exhibit size-dependent activity even after treatment at 450 °C, but the size-dependency disappears after calcination of PVP-stabilized Rh NPs.

Hydroformylation is also often used as a reaction system to explore dimensional regulation [108, 115, 116, 117]. Goodman et al. studied the structure-activity behavior of the $C_2H_4/CO/H_2$ reaction over Rh/SiO_2 catalysts with different Rh particle sizes [34]. C_2H_4 hydroformylation reactivity data was shown in Fig. 29. The particle size effect is easily observed, and maximal propionaldehyde TOF occurs near an average Rh particle diameter of about 2.5 nm. Their work also summarized two factors relevant to particle size dependence for the reaction: (i) an increase in propionaldehyde formation on undercoordinated Rh sites and (ii) creation of carbonyl hydride species (Rh(CO)H)) on smaller Rh particles.

2.4.2. Catalytic applications of shape-controlled Rh NPs

Most of the reactions catalyzed by Rh NPs are indeed structure-sensitive. Shape-controlled synthesis of Rh NPs has played an important role in enabling such studies

https://doi.org/10.1016/j.heliyon.2019.e01165

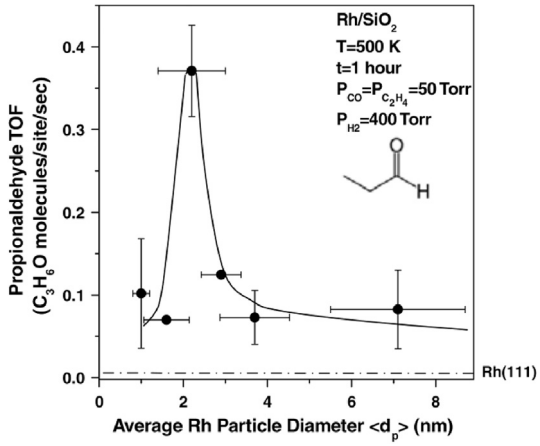

Fig. 29. Propionaldehyde TOF *vs.* average Rh particle size (nm). Reaction conditions: 50 Torr CO: 50 Torr C_2H_4: 400 Torr H_2 at T = 500 K for 1 h. $\pm\sigma_y$ error bars represent error of repeated reactivity measurements, $\pm\sigma_x$ error bars represent the sigma of the Rh particle size distribution as determined from STM measurements (Adapted with permission from [34]. Copyright 2011, the National Academy of Sciences of the United States of America).

by selectively exposing a specific type of facet on the surface, so that Rh NPs of different shapes can be used for different catalytic reactions [42].

Son et al. reported the different performances of two morphological (tetrahedral and spherical) Rh NPs in hydrogenation reaction [46]. For the hydrogenation of anthracene, three main products are formed in the hydrogenation reaction, including those produced by hydrogenation of the central ring (B), the two side rings (D), or only one side ring (C). As shown in Table 3, Rh nanotetrahedra on charcoal show obviously better catalytic effect than that of spherical particles and commercial Rh/C, and with 5.8- (Table 3, entry 2 vs. entry 3) and 109-times (Table 3, entry 2 vs. entry 5) higher in activity for the hydrogenation of anthracene than spherical Rh NPs and commercial Rh/C catalyst, respectively.

Table 3. Comparison of catalytic activity and selectivity for Rh NPs supported on charcoal in the hydrogenation of anthracene (Adapted with permission from [46]. Copyright 2007, Wiley-VCH).[a]

Entry	Catalyst	Pressure (atm)	Time (h)	Conv. (%)	Selectivity		
					B	C	D
1	Tetrahedral Rh/C	10	0.5	100	0.7	0.0	99.3
2	Tetrahedral Rh/C	1	2	100	2.0	0.0	98.0
3	Spherical Rh/C	1	2	99.5	6.7	76.3	17.0
4	Commercial Rh/C	10	0.5	57.3	6.4	81.0	12.6
5	Commercial Rh/C	1	2	4.8	35.4	45.8	18.8

[a] Reaction conditions: 1.00 mmol of anthracene and 1 mol% of Rh/C (based on ICP analysis) in methanol at room temperature.

https://doi.org/10.1016/j.heliyon.2019.e01165

Electrochemical measurements can also be used to investigate the dependence of catalytic activity on the shape of Rh NPs. Sun et al. successfully synthesized tetrahexahedral (THH) Rh NPs which exhibited greatly enhanced catalytic activity over commercial Rh black catalyst for the electrooxidation of ethanol and CO [47]. Fig. 30 illustrates different electrochemical performances for Rh NPs synthesized by the electrochemical square-wave-potential (SWP) route, as well as irregular nanoparticles and commercial Rh black catalyst. This is evident in Fig. 30a that THH Rh NPs can promote the oxygen adsorption in the low potential region and larger electrochemically active surface area (ECSA). Fig. 30b shows a characteristic peak of CO oxidation on these catalysts. It can be clearly seen that the onset potential and peak potential of CO oxidation of THH Rh NPs are the lowest, which could be further explained that the THH Rh NPs with high-index facets are beneficial to CO oxidation. Fig. 30c about the linear sweep voltammograms (LSV) of ethanol oxidation demonstrates that the THH Rh NPs yield the highest electrocatalytic activity of 2.69 mA cm^{-2}, 6.9 times that of commercial Rh black catalyst. Long-term chronoampermetric (CA) measurements in Fig. 30d evaluate the catalytic activity of ethanol oxidation under continuous operating conditions. It turns out that the THH Rh NPs has higher catalytic activity than commercial Rh black catalyst over the whole time range measured by CA. Sun et al. also demonstrated the chemical stability of THH Rh NPs, further certifying their catalytic value.

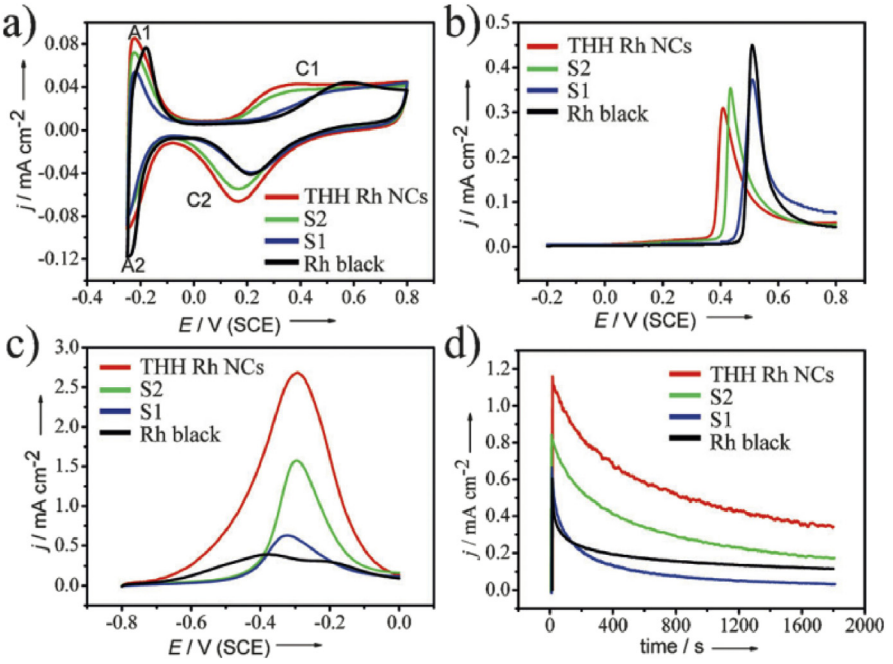

Fig. 30. Electrochemical characterization of as-synthesized Rh NPs, irregular nanoparticles and commercial Rh black catalyst: (a) cyclic voltammograms (CVs) in 0.1 M H_2SO_4 solution, (b) linear sweep voltammograms (LSV) of CO oxidation in 0.1 M H_2SO_4 solution, (c) LSVs of ethanol oxidation in 1.0 M ethanol + 1.0 M NaOH solution (scan rate: 50 mV s^{-1}), (d) current–time curves for ethanol oxidation at −0.45 V (Adapted with permission from [47]. Copyright 2014, Wiley-VCH).

https://doi.org/10.1016/j.heliyon.2019.e01165

3. Conclusions

Rh NPs have great influence on the production life and scientific research nowadays. Mastering the shape and size of Rh NPs can control their properties and enhance their usefulness for a given reaction. In this study, we aim at highlighting the wet chemistry-based methods in synthesizing Rh NPs, including the synthetic approaches and the specific controls for shape and size. Based on the accurate classification of various aspects of Rh, the key synthetic steps and control methods are expatiated. The influence of different shapes and sizes on various catalytic reactions provides a design basis for further industrial applications.

Even with these recent advancements in size- and shape-controlled Rh NPs, there are still many challenges in this important research field. Future research challenges in highly efficient Rh NPs may include: (i) to develop facile fabrication methods to precisely control the size and shape of Rh NPs and other NMNPs. Although the controlled preparation of Rh NPs has been studied a lot, its regulation and application are still restricted by the size and shape control compared with other platinum group metals such as Au, Ag, Pd, and Pt. Thus new synthetic approaches combined with existing control strategies for more Rh NPs with good control in sizes and shapes are sorely essential; (ii) to explore detailed characterization and mechanism. The further enhancement of theoretical simulation and in-situ characterization can reveal the mechanism behind synthesis and the interaction between compounds. This is conducive to guide the efficient synthesis of excellent metal nanomaterials; (iii) to reduce the amount of noble metals such as Rh. On the one hand, alternative catalysts can be found to replace noble metals; on the other hand, noble metals can be loaded on the substrates to improve their catalytic performance of unit precious metals.

These discoveries and proposals for Rh NPs are also applicable to other noble metal nanoparticles, and the ultimate goal of these studies is to apply more efficient catalysts for practical applications.

Declarations

Author contribution statement

All authors listed have significantly contributed to the development and the writing of this article.

Funding statement

This work was supported by the National Natural Science Foundation of China (Grant No.: 21506225, 21573240 and 21706265), and Center for Mesoscience,

https://doi.org/10.1016/j.heliyon.2019.e01165

Institute of Process Engineering, Chinese Academy of Sciences (Grant No.: COM2015A001 and MPCS-2017-A-02).

Competing interest statement

The authors declare no conflict of interest.

Additional information

No additional information is available for this paper.

References

[1] A.R. Tao, S. Habas, P. Yang, Shape control of colloidal metal nanocrystals, Small 4 (2008) 310–325.

[2] W. Niu, G. Xu, Crystallographic control of noble metal nanocrystals, Nano Today 6 (2011) 265–285.

[3] J.W. Hong, S.U. Lee, Y.W. Lee, S.W. Han, Hexoctahedral Au nanocrystals with high-index facets and their optical and surface-enhanced Raman scattering properties, J. Am. Chem. Soc. 134 (2012) 4565–4568.

[4] K. Zhou, Y. Li, Catalysis based on nanocrystals with well-defined facets, Angew. Chem. Int. Ed. 51 (2012) 602–613.

[5] J. Wu, H. Yang, Platinum-based oxygen reduction electrocatalysts, Acc. Chem. Res. 46 (2013) 1848–1857.

[6] S. Xie, S.-I. Choi, X. Xia, Y. Xia, Catalysis on faceted noble-metal nanocrystals: both shape and size matter, Curr. Opin. Chem. Eng. 2 (2013) 142–150.

[7] W. Zang, G. Li, L. Wang, X. Zhang, Catalytic hydrogenation by noble-metal nanocrystals with well-defined facets: a review, Catal. Sci. Technol. 5 (2015) 2532–2553.

[8] J.L. Elechiguerra, J.L. Burt, J.R. Morones, A. Camacho-Bragado, X. Gao, H.H. Lara, M.J. Yacaman, Interaction of silver nanoparticles with HIV-1, J. Nanobiotechnol. 3 (2005) 6–15.

[9] B.T. Sneed, C.H. Kuo, C.N. Brodsky, C.K. Tsung, Iodide-mediated control of rhodium epitaxial growth on well-defined noble metal nanocrystals: synthesis, characterization, and structure-dependent catalytic properties, J. Am. Chem. Soc. 134 (2012) 18417–18426.

https://doi.org/10.1016/j.heliyon.2019.e01165

[10] K.D. Gilroy, A. Ruditskiy, H.C. Peng, D. Qin, Y. Xia, Bimetallic nanocrystals: syntheses, properties, and applications, Chem. Rev. 116 (2016) 10414−10472.

[11] C. Wang, H. Daimon, T. Onodera, T. Koda, S. Sun, A general approach to the size- and shape-controlled synthesis of platinum nanoparticles and their catalytic reduction of oxygen, Angew. Chem. Int. Ed. 47 (2008) 3588−3591.

[12] G. Kyriakou, S.K. Beaumont, S.M. Humphrey, C. Antonetti, R.M. Lambert, Sonogashira coupling catalyzed by gold nanoparticles: does homogeneous or heterogeneous catalysis dominate? ChemCatChem 2 (2010) 1444−1449.

[13] C. Campbell, S. Parker, D. Starr, The effect of size-dependent nanoparticle energetics on catalyst sintering, Science 298 (2002) 811−814.

[14] S.H. Joo, J.Y. Park, J.R. Renzas, D.R. Butcher, W. Huang, G.A. Somorjai, Size effect of ruthenium nanoparticles in catalytic carbon monoxide oxidation, Nano Lett. 10 (2010) 2709−2713.

[15] N. Zettsu, J.M. McLellan, B. Wiley, Y. Yin, Z.-Y. Li, Y. Xia, Synthesis, stability, and surface plasmonic properties of rhodium multipods, and their use as substrates for surface-enhanced Raman scattering, Angew. Chem. Int. Ed. 45 (2006) 1288−1292.

[16] J. Zhang, H. Yang, J. Fang, S. Zou, Synthesis and oxygen reduction activity of shape-controlled Pt3Ni nanopolyhedra, Nano Lett. 10 (2010) 638−644.

[17] I. Lee, F. Delbecq, R. Morales, M.A. Albiter, F. Zaera, Tuning selectivity in catalysis by controlling particle shape, Nat. Mater. 8 (2009) 132−138.

[18] C.-K. Tsung, J.N. Kuhn, W. Huang, C. Aliaga, L.-I. Hung, G.A. Somorjai, P. Yang, Sub-10 nm platinum nanocrystals with size and shape control: catalytic study for ethylene and pyrrole hydrogenation, J. Am. Chem. Soc. 131 (2009) 5816−5822.

[19] G.A. Somorjai, D.W. Blakely, Mechanism of catalysis of hydrocarbon reactions by platinum surfaces, Nature 258 (1975) 580−583.

[20] N. Tian, Z. Zhou, S. Sun, Y. Ding, Z. Wang, Synthesis of tetrahexahedral platinum nanocrystals with high-index facets and high electro-oxidation activity, Science 316 (2007) 732−735.

[21] A.J. Biacchi, R.E. Schaak, The solvent matters: kinetic versus thermodynamic shape control in the polyol synthesis of rhodium nanoparticles, ACS Nano 5 (2011) 8089−8099.

https://doi.org/10.1016/j.heliyon.2019.e01165

[22] M.E. Grass, Y. Zhang, D.R. Butcher, J.Y. Park, Y. Li, H. Bluhm, K.M. Bratlie, T. Zhang, G.A. Somorjai, A reactive oxide overlayer on rhodium nanoparticles during CO oxidation and its size dependence studied by in situ ambient-pressure X-ray photoelectron spectroscopy, Angew. Chem. Int. Ed. 47 (2008) 8893−8896.

[23] J. Gustafson, R. Westerström, A. Mikkelsen, X. Torrelles, O. Balmes, N. Bovet, J.N. Andersen, C.J. Baddeley, E. Lundgren, Sensitivity of catalysis to surface structure: the example of CO oxidation on Rh under realistic conditions, Phys. Rev. B 78 (2008) 045423.

[24] R. Wang, H. He, J. Wang, L. Liu, H. Dai, Shape-regulation: an effective way to control CO oxidation activity over noble metal catalysts, Catal. Today 201 (2013) 68−78.

[25] Y. Zhang, M.E. Grass, W. Huang, G.A. Somorjai, Seedless polyol synthesis and CO oxidation activity of monodisperse (111)- and (100)-oriented rhodium nanocrystals in sub-10 nm sizes, Langmuir 26 (2010) 16463−16468.

[26] H.S. Gandhi, G.W. Graham, R.W. McCabe, Automotive exhaust catalysis, J. Catal. 216 (2003) 433−442.

[27] J.R. Renzas, Y. Zhang, W. Huang, G.A. Somorjai, Rhodium nanoparticle shape dependence in the reduction of NO by CO, Catal. Lett. 132 (2009) 317−322.

[28] J.H. Holles, M.A. Switzer, R.J. Davis, Influence of ceria and lanthana promoters on the kinetics of NO and N_2O reduction by CO over alumina-supported palladium and rhodium, J. Catal. 190 (2000) 247−260.

[29] Y. Yuan, N. Yan, P.J. Dyson, Advances in the rational design of rhodium nanoparticle catalysts: control via manipulation of the nanoparticle core and stabilizer, ACS Catal. 2 (2012) 1057−1069.

[30] D.K. Liguras, D.I. Kondarides, X.E. Verykios, Production of hydrogen for fuel cells by steam reforming of ethanol over supported noble metal catalysts, Appl. Catal. B Environ. 43 (2003) 345−354.

[31] X.-Y. Quek, Y. Guan, E.J.M. Hensen, Structure sensitivity in the hydrogenation of unsaturated hydrocarbons over Rh nanoparticles, Catal. Today 183 (2012) 72−78.

[32] M.J. Jacinto, P.K. Kiyohara, S.H. Masunaga, R.F. Jardim, L.M. Rossi, Recoverable rhodium nanoparticles: synthesis, characterization and catalytic

https://doi.org/10.1016/j.heliyon.2019.e01165

performance in hydrogenation reactions, Appl. Catal. A Gen. 338 (2008) 52−57.

[33] V. Cimpeanu, M. Kocevar, V.I. Parvulescu, W. Leitner, Preparation of rhodium nanoparticles in carbon dioxide induced ionic liquids and their application to selective hydrogenation, Angew. Chem. Int. Ed. 48 (2009) 1085−1088.

[34] S.M. McClure, M.J. Lundwall, D.W. Goodman, Planar oxide supported rhodium nanoparticles as model catalysts, Proc. Natl. Acad. Sci. U. S. A. 108 (2011) 931−936.

[35] T.-J. Yoon, J.I. Kim, J.-K. Lee, Rh-based olefin hydroformylation catalysts and the change of their catalytic activity depending on the size of immobilizing supporters, Inorg. Chim. Acta 345 (2003) 228−234.

[36] C. Hou, G. Zhao, Y. Ji, Z. Niu, D. Wang, Y. Li, Hydroformylation of alkenes over rhodium supported on the metal-organic framework ZIF-8, Nano Res. 7 (2014) 1364−1369.

[37] Y. Zhang, M. Janyasupab, C.-W. Liu, X. Li, J. Xu, C.-C. Liu, Three dimensional PtRh alloy porous nanostructures: tuning the atomic composition and controlling the morphology for the application of direct methanol fuel cells, Adv. Funct. Mater. 22 (2012) 3570−3575.

[38] B.R. Sathe, B.K. Balan, V.K. Pillai, Enhanced electrocatalytic performance of interconnected Rh nano-chains towards formic acid oxidation, Energy Environ. Sci. 4 (2011) 1029−1036.

[39] Y. Suo, I.M. Hsing, Highly active rhodium/carbon nanocatalysts for ethanol oxidation in alkaline medium, J. Power Sources 196 (2011) 7945−7950.

[40] B.R. Sathe, D.B. Shinde, V.K. Pillai, Preparation and characterization of rhodium nanostructures through the evolution of microgalvanic cells and their enhanced electrocatalytic activity for formaldehyde oxidation, J. Phys. Chem. C 113 (2009) 9616−9622.

[41] S.-I. Choi, S.R. Lee, C. Ma, B. Oliy, M. Luo, M. Chi, Y. Xia, Facile synthesis of rhodium icosahedra with controlled sizes up to 12 nm, ChemNanoMat 2 (2016) 61−66.

[42] S. Xie, X.Y. Liu, Y. Xia, Shape-controlled syntheses of rhodium nanocrystals for the enhancement of their catalytic properties, Nano Res. 8 (2015) 82−96.

[43] Y. Zhang, M.E. Grass, J.N. Kuhn, F. Tao, S.E. Habas, W. Huang, P. Yang, G.A. Somorjai, Highly selective synthesis of cataytically active monodisperse rhodium nanocubes, J. Am. Chem. Soc. 130 (2008) 5868−5869.

https://doi.org/10.1016/j.heliyon.2019.e01165

[44] J. Hoefelmeyer, K. Niesz, G. Somorjai, T. Tilley, Radial anisotropic growth of rhodium nanoparticles, Nano Lett. 5 (2005) 435−438.

[45] S.M. Humphrey, M.E. Grass, S.E. Habas, K. Niesz, G.A. Somorjai, T.D. Tilley, Rhodium nanoparticles from cluster seeds: control of size and shape by precursor addition rate, Nano Lett. 7 (2007) 785−790.

[46] K.H. Park, K. Jang, H.J. Kim, S.U. Son, Near-monodisperse tetrahedral rhodium nanoparticles on charcoal: the shape-dependent catalytic hydrogenation of arenes, Angew. Chem. Int. Ed. 46 (2007) 1152−1155.

[47] N.F. Yu, N. Tian, Z.Y. Zhou, L. Huang, J. Xiao, Y.H. Wen, S.G. Sun, Electrochemical synthesis of tetrahexahedral rhodium nanocrystals with extraordinarily high surface energy and high electrocatalytic activity, Angew. Chem. Int. Ed. 53 (2014) 5097−5101.

[48] S. Xie, N. Lu, Z. Xie, J. Wang, M.J. Kim, Y. Xia, Synthesis of Pd-Rh core-frame concave nanocubes and their conversion to Rh cubic nanoframes by selective etching of the Pd cores, Angew. Chem. Int. Ed. 51 (2012) 10266−10270.

[49] K.N. Avery, J.E. Schaak, R.E. Schaak, M13 bacteriophage as a biological scaffold for magnetically-recoverable metal nanowire catalysts: combining specific and nonspecific interactions to design multifunctional nanocomposites, Chem. Mater. 21 (2009) 2176−2178.

[50] Y. Sun, Y. Xia, Shape-controlled synthesis of gold and silver nanoparticles, Science 298 (2002) 2176−2179.

[51] W. Cai, J. Wan, Facile synthesis of superparamagnetic magnetite nanoparticles in liquid polyols, J. Colloid Interface Sci. 305 (2007) 366−370.

[52] K.H. Park, S.H. Im, O.O. Park, The size control of silver nanocrystals with different polyols and its application to low-reflection coating materials, Nanotechnology 22 (2011) 045602.

[53] K.J. Carroll, J.U. Reveles, M.D. Shultz, S.N. Khanna, E.E. Carpenter, Preparation of elemental Cu and Ni nanoparticles by the polyol method: an experimental and theoretical approach, J. Phys. Chem. C 115 (2011) 2656−2664.

[54] K.M. Koczkur, S. Mourdikoudis, L. Polavarapu, S.E. Skrabalak, Polyvinylpyrrolidone (PVP) in nanoparticle synthesis, Dalton Trans. 44 (2015) 17883−17905.

[55] H. Wang, S. Zhou, K.D. Gilroy, Z. Cai, Y. Xia, Icosahedral nanocrystals of noble metals: synthesis and applications, Nano Today 15 (2017) 121−144.

https://doi.org/10.1016/j.heliyon.2019.e01165

[56] A. Tuchscherer, R. Packheiser, T. Rüffer, H. Schletter, M. Hietschold, H. Lang, Rhodium nanoparticles from dirhodium(II) ethylene glycol tetracarboxylates, Eur. J. Inorg. Chem. 13 (2012) 2251−2258.

[57] H. Hirai, Y. Nakao, N. Toshima, Preparation of colloidal rhodium in poly(-vinyl Alcohol) by reduction with methanol, J. Macromol. Sci. Part A Pure Appl. Chem. 12 (1978) 1117−1141.

[58] A.J. Biacchi, R.E. Schaak, Ligand-induced fate of embryonic species in the shape-controlled synthesis of rhodium nanoparticles, ACS Nano 9 (2015) 1707−1720.

[59] N. Dahal, S. Garcia, J. Zhou, S.M. Humphrey, Beneficial effects of microwave-assisted heating versus conventional heating in noble metal nanoparticle synthesis, ACS Nano 6 (2012) 9433−9446.

[60] H. Yu, P. Gibbons, K. Kelton, W. Buhro, Heterogeneous seeded growth: a potentially general synthesis of monodisperse metallic nanoparticles, J. Am. Chem. Soc. 123 (2001) 9198−9199.

[61] K. Mallick, Z. Wang, T. Pal, Seed-mediated successive growth of gold particles accomplished by UV irradiation: a photochemical approach for size-controlled synthesis, J. Photochem. Photobiol. A Chem. 140 (2001) 75−80.

[62] F. Jutz, J.-M. Andanson, A. Baiker, A green pathway for hydrogenations on ionic liquid-stabilized nanoparticles, J. Catal. 268 (2009) 356−366.

[63] F. Hoxha, N. Vanvegten, A. Urakawa, F. Krumeich, T. Mallat, A. Baiker, Remarkable particle size effect in Rh-catalyzed enantioselective hydrogenations, J. Catal. 261 (2009) 224−231.

[64] J.K. Norskov, T. Bligaard, B. Hvolbaek, F. Abild-Pedersen, I. Chorkendorff, C.H. Christensen, The nature of the active site in heterogeneous metal catalysis, Chem. Soc. Rev. 37 (2008) 2163−2171.

[65] R.A. Van Santen, Complementary structure sensitive and insensitive catalytic relationships, Acc. Chem. Res. 42 (2009) 57−66.

[66] X. Zhang, P. Li, Á. Barreda, Y. Gutiérrez, F. González, F. Moreno, H.O. Everitt, J. Liu, Size-tunable rhodium nanostructures for wavelength-tunable ultraviolet plasmonics, Nanoscale Horiz. 1 (2016) 75−80.

[67] R. Narayanan, M.A. El-Sayed, Effect of catalysis on the stability of metallic nanoparticles: suzuki reaction catalyzed by PVP-palladium nanoparticles, J. Am. Chem. Soc. 125 (2003) 8340−8347.

https://doi.org/10.1016/j.heliyon.2019.e01165

[68] J.Y. Park, Y. Zhang, M. Grass, T. Zhang, G.A. Somorjai, Tuning of catalytic CO oxidation by changing composition of Rh-Pt bimetallic nanoparticles, Nano Lett. 8 (2008) 673−677.

[69] A. Gual, C. Godard, K. Philippot, B. Chaudret, A. Denicourt-Nowicki, A. Roucoux, S. Castillon, C. Claver, Carbohydrate-derived 1,3-diphosphite ligands as chiral nanoparticle stabilizers: promising catalytic systems for asymmetric hydrogenation, ChemSusChem 2 (2009) 769−779.

[70] A. Gual, C. Godard, C. Claver, S. Castillón, C1-symmetric diphosphite ligands derived from carbohydrates: influence of structural modifications on the rhodium-catalyzed asymmetric hydroformylation of styrene, Eur. J. Org. Chem. 8 (2009) 1191−1201.

[71] S. Yao, Y. Yuan, C. Xiao, W. Li, Y. Kou, P.J. Dyson, N. Yan, H. Asakura, K. Teramura, T. Tanaka, Insights into the formation mechanism of rhodium nanocubes, J. Phys. Chem. C 116 (2012) 15076−15086.

[72] H. Zhang, W. Li, M. Jin, J. Zeng, T. Yu, D. Yang, Y. Xia, Controlling the morphology of rhodium nanocrystals by manipulating the growth kinetics with a syringe pump, Nano Lett. 11 (2011) 898−903.

[73] S.R. Lee, M. Vara, Z.D. Hood, M. Zhao, K.D. Gilroy, M. Chi, Y. Xia, Rhodium decahedral nanocrystals: facile synthesis, mechanistic insights, and experimental controls, ChemNanoMat 4 (2018) 66−70.

[74] N.V. Long, N.D. Chien, H. Hirata, T. Matsubara, M. Ohtaki, M. Nogami, Highly monodisperse cubic and octahedral rhodium nanocrystals: their evolutions from sharp polyhedrons into branched nanostructures and surface-enhanced Raman scattering, J. Cryst. Growth 320 (2011) 78−89.

[75] T. Ewers, A. Sra, B. Norris, R. Cable, C. Cheng, D. Shantz, R. Schaak, Spontaneous hierarchical assembly of rhodium nanoparticles into spherical aggregates and superlattices, Chem. Mater. 17 (2005) 514−520.

[76] Q. Yuan, Z. Zhou, J. Zhuang, X. Wang, Tunable aqueous phase synthesis and shape-dependent electrochemical properties of rhodium nanostructures, Inorg. Chem. 49 (2010) 5515−5521.

[77] H. Zhang, X. Xia, W. Li, J. Zeng, Y. Dai, D. Yang, Y. Xia, Facile synthesis of five-fold twinned, starfish-like rhodium nanocrystals by eliminating oxidative etching with a chloride-free precursor, Angew. Chem. Int. Ed. 49 (2010) 5296−5300.

[78] K. Jang, H.J. Kim, S.U. Son, Low-temperature synthesis of ultrathin rhodium nanoplates via molecular orbital symmetry interaction between rhodium precursors, Chem. Mater. 22 (2010) 1273−1275.

https://doi.org/10.1016/j.heliyon.2019.e01165

[79] H. Duan, N. Yan, R. Yu, C.R. Chang, G. Zhou, H.S. Hu, H. Rong, Z. Niu, J. Mao, H. Asakura, T. Tanaka, P.J. Dyson, J. Li, Y. Li, Ultrathin rhodium nanosheets, Nat. Commun. 5 (2014) 3093.

[80] Y. Zheng, J. Zeng, A. Ruditskiy, M. Liu, Y. Xia, Oxidative etching and its role in manipulating the nucleation and growth of noble-metal nanocrystals, Chem. Mater. 26 (2013) 22−33.

[81] Y. Feng, X. Ma, L. Han, Z. Peng, J. Yang, A universal approach to the synthesis of nanodendrites of noble metals, Nanoscale 6 (2014) 6173−6179.

[82] S. Mourdikoudis, L.M. Liz-Marzán, Oleylamine in nanoparticle synthesis, Chem. Mater. 25 (2013) 1465−1476.

[83] H. Hiramatsu, F.E. Osterloh, A simple large-scale synthesis of nearly monodisperse gold and silver nanoparticles with adjustable sizes and with exchangeable surfactants, Chem. Mater. 16 (2004) 2509−2511.

[84] H. Yu, M. Chen, P.M. Rice, S.X. Wang, R.L. White, S. Sun, Dumbbell-like bifunctional Au-Fe_3O_4 nanoparticles, Nano Lett. 5 (2005) 379−382.

[85] Z. Li, J. Tao, X. Lu, Y. Zhu, Y. Xia, Facile synthesis of ultrathin Au nanorods by aging the AuCl(oleylamine) complex with amorphous Fe nanoparticles in chloroform, Nano Lett. 8 (2008) 3052−3055.

[86] Z. Xu, C. Shen, Y. Hou, H. Cao, S. Sun, Oleylamine as both reducing agent and stabilizer in a facile synthesis of magnetite nanoparticles, Chem. Mater. 21 (2009) 1778−1780.

[87] X. Liu, M. Atwater, J. Wang, Q. Dai, J. Zou, J.P. Brennan, Q. Huo, A study on gold nanoparticle synthesis using oleylamine as both reducing agent and protecting ligand, J. Nanosci. Nanotechnol. 7 (2007) 3126−3133.

[88] M.R. Langille, M.L. Personick, J. Zhang, C.A. Mirkin, Defining rules for the shape evolution of gold nanoparticles, J. Am. Chem. Soc. 134 (2012) 14542−14554.

[89] H. Zhang, M. Jin, Y. Xia, Noble-metal nanocrystals with concave surfaces: synthesis and applications, Angew. Chem. Int. Ed. 51 (2012) 7656−7673.

[90] S. Xie, H. Zhang, N. Lu, M. Jin, J. Wang, M.J. Kim, Z. Xie, Y. Xia, Synthesis of rhodium concave tetrahedrons by collectively manipulating the reduction kinetics, facet-selective capping, and surface diffusion, Nano Lett. 13 (2013) 6262−6268.

[91] Y. Chen, Q.S. Chen, S.Y. Peng, Z.Q. Wang, G. Lu, G.C. Guo, Manipulating the concavity of rhodium nanocubes enclosed by high-index facets via site-selective etching, Chem. Commun. 50 (2014) 1662−1664.

https://doi.org/10.1016/j.heliyon.2019.e01165

[92] Y. Bi, G. Lu, Iodide ions control galvanic replacement growth of uniform rhodium nanotubes at room temperature, Chem. Commun. 47 (2008) 6402–6404.

[93] R. Franke, D. Selent, A. Borner, Applied hydroformylation, Chem. Rev. 112 (2012) 5675–5732.

[94] X. Huang, Z. Zhao, Y. Chen, C.-Y. Chiu, L. Ruan, Y. Liu, M. Li, X. Duan, Y. Huang, High density catalytic hot spots in ultrafine wavy nanowires, Nano Lett. 14 (2014) 3887–3894.

[95] M. Shelef, G.W. Graham, Why rhodium in automotive three-way catalysts? Catal. Rev. 36 (2006) 433–457.

[96] A.M. Watson, X. Zhang, R.A. de la Osa, J.M. Sanz, F. González, F. Moreno, G. Finkelstein, J. Liu, H.O. Everitt, Rhodium nanoparticles for ultraviolet plasmonics, Nano Lett. 15 (2015) 1095–1100.

[97] R.A. de la Osa, J.M. Sanz, A.I. Barreda, J.M. Saiz, F. González, H.O. Everitt, F. Moreno, Rhodium tripod stars for UV plasmonics, J. Phys. Chem. C 119 (2015) 12572–12580.

[98] K. Li, Y. Wang, J. Jiang, Z. Jin, Thermoregulated phase-transfer rhodium nanoparticle catalyst for hydrogenation in an aqueous/organic biphasic system, Catal. Commun. 11 (2010) 542–546.

[99] A. Gniewek, A.M. Trzeciak, Rh(0) nanoparticles: synthesis, structure and catalytic application in Suzuki–Miyaura reaction and hydrogenation of benzene, Top. Catal. 56 (2013) 1239–1245.

[100] E.W. Harak, K.M. Koczkur, D.W. Harak, P. Patton, S.E. Skrabalak, Designing efficient catalysts through bimetallic architecture: Rh@Pt nanocubes as a case study, ChemNanoMat 3 (2017) 815–821.

[101] Z.Y. Zhou, N. Tian, J.T. Li, I. Broadwell, S.G. Sun, Nanomaterials of high surface energy with exceptional properties in catalysis and energy storage, Chem. Soc. Rev. 40 (2011) 4167–4185.

[102] F. Zaera, Shape-controlled nanostructures in heterogeneous catalysis, ChemSusChem 6 (2013) 1797–1820.

[103] F.C. Campos-Skrobot, R.C.P. Rizzo-Domingues, N.R.C. Fernandes-Machado, M.P. Cantão, Novel zeolite-supported rhodium catalysts for ethanol steam reforming, J. Power Sources 183 (2008) 713–716.

[104] H.-B. Pan, C.M. Wai, One-step synthesis of size-tunable rhodium nanoparticles on carbon nanotubes: a study of particle size effect on hydrogenation of xylene, J. Phys. Chem. C 114 (2010) 11364–11369.

https://doi.org/10.1016/j.heliyon.2019.e01165

[105] V.K. Kanuru, S.M. Humphrey, J.M. Kyffin, D.A. Jefferson, J.W. Burton, M. Armbruster, R.M. Lambert, Evidence for heterogeneous sonogashira coupling of phenylacetylene and iodobenzene catalyzed by well defined rhodium nanoparticles, Dalton Trans. 37 (2009) 7602−7605.

[106] D.A. Ligthart, R.A. van Santen, E.J. Hensen, Supported rhodium oxide nanoparticles as highly active CO oxidation catalysts, Angew. Chem. Int. Ed. 50 (2011) 5306−5310.

[107] D.A.J.M. Ligthart, R.A. van Santen, E.J.M. Hensen, Influence of particle size on the activity and stability in steam methane reforming of supported Rh nanoparticles, J. Catal. 280 (2011) 206−220.

[108] D. Han, X. Li, H. Zhang, Z. Liu, J. Li, C. Li, Heterogeneous asymmetric hydroformylation of olefins on chirally modified Rh/SiO_2 catalysts, J. Catal. 243 (2006) 318−328.

[109] A. Siani, O.S. Alexeev, D. Samuel Deutsch, J.R. Monnier, P.T. Fanson, H. Hirata, S. Matsumoto, C.T. Williams, M.D. Amiridis, Dendrimer-mediated synthesis of subnanometer-sized Rh particles supported on ZrO_2, J. Catal. 266 (2009) 331−342.

[110] E.G. Bilé, R. Sassine, A. Denicourt-Nowicki, F. Launay, A. Roucoux, New ammonium surfactant-stabilized rhodium(0) colloidal suspensions: influence of novel counter-anions on physico-chemical and catalytic properties, Dalton Trans. 40 (2011) 6524−6531.

[111] K. Hindle, S. Jackson, D. Stirling, G. Webb, The hydrogenation of para-toluidine over rhodium/silica: the effect of metal particle size and support texture, J. Catal. 241 (2006) 417−425.

[112] N. Kapur, J. Hyun, B. Shan, J.B. Nicholas, K. Cho, Ab initio study of CO hydrogenation to oxygenates on reduced Rh terraces and stepped surfaces, J. Phys. Chem. C 114 (2010) 10171−10182.

[113] Y. Zhang, M.E. Grass, S.E. Habas, F. Tao, T. Zhang, P. Yang, G.A. Somorjai, One-step polyol synthesis and Langmuir-blodgett monolayer formation of size-tunable monodisperse rhodium nanocrystals with catalytically active (111) surface structures, J. Phys. Chem. C 111 (2007) 12243−12253.

[114] P. Jacobs, G. Somorjai, Conversion of heterogeneous catalysis from art to science: the surface science of heterogeneous catalysis, J. Mol. Catal. A Chem. 131 (1998) 5−18.

https://doi.org/10.1016/j.heliyon.2019.e01165

[115] A.J. Bruss, M.A. Gelesky, G. Machado, J. Dupont, Rh(0) nanoparticles as catalyst precursors for the solventless hydroformylation of olefins, J. Mol. Catal. A Chem. 252 (2006) 212–218.

[116] L. Yan, Y.J. Ding, L.W. Lin, H.J. Zhu, H.M. Yin, X.M. Li, Y. Lu, In situ formation of $HRh(CO)_2(PPh3)_2$ active species on the surface of a SBA-15 supported heterogeneous catalyst and the effect of support pore size on the hydroformylation of propene, J. Mol. Catal. A Chem. 300 (2009) 116–120.

[117] M.R. Axet, S. Castillón, C. Claver, K. Philippot, P. Lecante, B. Chaudret, Chiral diphosphite-modified rhodium(0) nanoparticles: catalyst reservoir for styrene hydroformylation, Eur. J. Inorg. Chem. 22 (2008) 3460–3466.

https://doi.org/10.1016/j.heliyon.2019.e01165